

NACA RM L52D18a

7323



NACA

RESEARCH MEMORANDUM

LARGE-SCALE FLIGHT MEASUREMENTS OF ZERO-LIFT DRAG OF
10 WING-BODY CONFIGURATIONS AT MACH
NUMBERS FROM 0.8 TO 1.6

By John D. Morrow and Robert L. Nelson

Langley Aeronautical Laboratory
Langley Field, Va.

NATIONAL ADVISORY COMMITTEE
FOR AERONAUTICS

WASHINGTON
January 15, 1953

Classification (or changed to) UNCLASSIFIED

By Authority of NASA Tech. Performance Ment. #1
(OFFICER AUTHORIZED TO CHANGE)

By 4 Nov 57
NAME AND

WMA
GRADE OF OFFICER MAKING CHANGE)

30 Mar 51
DATE



NATIONAL ADVISORY COMMITTEE FOR AERONAUTICS

RESEARCH MEMORANDUM

LARGE-SCALE FLIGHT MEASUREMENTS OF ZERO-LIFT DRAG OF

10 WING-BODY CONFIGURATIONS AT MACH

NUMBERS FROM 0.8 TO 1.6

By John D. Morrow and Robert L. Nelson

SUMMARY

Ten large-scale rocket-propelled wing-body configurations have been flown by the Pilotless Aircraft Research Division at Mach numbers from 0.8 to 1.6 and Reynolds numbers up to 50×10^6 , based on the mean aerodynamic chord of the wing. In general, the wings had straight, sweptback, or triangular plan forms and thickness ratios from 3 to 12 percent. They were mounted on bodies of fineness ratio 10, with frontal areas of 3 to 6 percent of the wing plan form areas. The results include zero-lift drag, base pressure, and estimates of maximum lift-drag ratios.

Of several wing-body configurations having straight, swept, and delta wings of equal area, a 3-percent-thick, 60° delta wing had the least zero-lift drag at supersonic speeds. At transonic speeds, however, a 5.6-percent-thick swept wing had the least drag. At low supersonic speeds the maximum lift-drag ratios for all models were between 7 and 9.5. Changing the section of a straight wing from a hexagonal section to an NACA 65A004.5 section resulted in a 23-percent reduction in zero-lift drag coefficient at transonic speeds. At higher speeds, the drag difference decreased, and it was zero at $M = 1.4$. Doubling the thickness of the 3-percent-thick, 60° delta wing added roughly 40 percent to the configuration drag and 60 percent to the wing drag at zero lift. Differences in body profile shape had a large effect on the interference drag of a wing-body combination at transonic speeds, but were of little significance at subsonic and supersonic speeds for the specific bodies studied in this investigation. The base pressures on the bodies of the present configurations indicate base drags of very small magnitude. The pressures were affected by the size and shape of the wings mounted on the body.

INTRODUCTION

A program of research is being conducted by the National Advisory Committee for Aeronautics which is directed toward the development of aircraft configurations suitable for efficient flight at transonic and supersonic speeds. This paper presents the zero-lift drag and base pressure results obtained on eleven wing-body models (ten configurations) and four wingless models (two configurations) in free flight and at large Reynolds numbers. Some of the results have been presented previously in references 1 to 7. The main variable in the tests was wing configuration; however, the body shape was varied for one wing configuration. Also, identical configurations were tested with two surface finishes. The tests covered a Mach number range from 0.8 to 1.6 which corresponds to a Reynolds number range of 7.5×10^6 to 50×10^6 , based on the mean aerodynamic chord of the wing.

SYMBOLS

C_D	drag coefficient at zero lift, Drag/qS_w
C_{p_b}	body base pressure coefficient, $\frac{p_b - p_o}{q}$
p_b	body base pressure, lb/sq ft
p_o	atmospheric pressure, lb/sq ft
q	dynamic pressure, $\frac{1}{2}\rho V^2$, lb/sq ft
M	Mach number
R	test Reynolds number
ρ	air density, slugs/cu ft
V	air velocity, ft/sec
Λ	wing sweepback angle
A	wing aspect ratio, b^2/S_w
λ	wing taper ratio, c_t/c_r

b	wing span
y	spanwise distance from body center line
c	wing local chord
c_r	wing root chord
c_t	wing tip chord
t	wing local thickness

$(t/c)_{rms}$	wing root-mean-square thickness ratio,	$\sqrt{\frac{\int_0^{b/2} (t/c)^2 c \, dy}{\int_0^{b/2} c \, dy}}$
---------------	--	--

S_w	wing plan-form area to center line of model, sq ft
S_f	body frontal area, 0.922 sq ft
S_e	exposed wing area, sq ft

$(L/D)_{max}$	maximum lift-drag ratio,	$\frac{1}{2} \sqrt{\frac{1}{(dC_D/dC_L^2) C_D}}$
---------------	--------------------------	--

dC_D/dC_L^2	drag-due-to-lift parameter
---------------	----------------------------

C_L	coefficient of lift, Lift/ qS_w
-------	-----------------------------------

MODELS AND TESTS

The general arrangement and basic geometry of the tested configurations are given in figure 1 and table I. The ordinates of the two body shapes used in the present tests are given in table II. Both body shapes had a fineness ratio of 10, frontal area of 0.922 square foot, and base area of 0.228 square foot. The parabolic body had a profile defined by two parabolic arcs, each having its vertex at the maximum diameter, which was located at the 40-percent station of the body. The transonic body had an arbitrary profile which placed the maximum diameter at the 60-percent station of the body; this shape was the basic one used

in the NACA transonic research program. For each model, the wing was so located that the quarter-chord point of the mean aerodynamic chord fell at the 60-percent station of the body.

The models had thin sweptback tail fins, four on the wingless models and two on the winged models. A typical fin is shown in figure 2. The drag contribution of the stabilizing fins was determined from separate tests by the drag-measurement technique of reference 8. The test vehicle used to measure the fin drag is shown in figure 3.

The models were constructed primarily of wood and reinforced with metal. All of the models except 1(a), 6(a), 7, and 11(a) were finished with clear lacquer and polished to form a smooth glossy surface. Models 7 and 11(a) were finished with orange lacquer. Models 1(a) and 6(a) were finished with a compound of zinc stearate and plastic glue which resulted in a smooth nonglossy surface. There appeared to be no significant differences in the smoothness of the surfaces. No measurements were made of surface roughness.

An ABL Deacon 6-inch rocket motor with a total impulse of 19,000 pound-seconds, contained within the bodies, propelled the models to supersonic speeds. The models were launched as shown in figure 4 at an angle of approximately 65° .

For all test models, a telemeter was contained within the body to measure longitudinal acceleration and base pressure. The telemeter of model 5 measured normal accelerations in addition to the two above-mentioned quantities. No base pressure measurements were made on model 10. Ground instruments were also used to record the model flights; they consisted of a CW Doppler velocimeter for measuring velocity, an NACA modified SCR 584 radar tracking unit for measuring trajectory, and radiosondes for measuring air pressure, density, and temperature. The data which are presented were measured during the coasting period of the flights after the rocket propellant had been exhausted. The total drag was obtained by two independent methods: direct measurement of longitudinal acceleration from the telemeter and the differentiation of the velocity-time curve (obtained from the CW Doppler velocimeter). Base pressure coefficients were determined from the radiosonde survey of ambient pressures and telemetered values of pressure at the periphery of the base. Details of the base pressure orifice installation are shown in figure 5.

Wind velocities for each model have been estimated by the Meteorology Unit of the Langley Flight Research Division by using winds-aloft data obtained at nearby weather stations. Winds at altitude, estimated in this manner, agree well with recently measured winds obtained by tracking radiosonde balloons. The wind velocities have been added vectorially to the ground velocities from the Doppler radar to obtain air velocity.

The drag results are subject to the following errors: (1) errors in the measurement of longitudinal acceleration, (2) errors in drag coefficient and Mach number mainly due to errors in the estimated wind, and (3) errors due to rocket-motor afterburning. Figure 6 presents the basic drag data for a typical configuration. The error in the measured longitudinal acceleration is indicated by the difference between Doppler and telemeter drag-coefficient test points at a given Mach number. The greatest difference between Doppler and telemeter drag data for this model occurs at transonic speeds and results from the method of obtaining accelerations from Doppler velocity data. The Doppler accelerations are obtained by taking the slope of the velocity-time curve over a given time interval. When rapid changes in acceleration occur within this time interval, the accelerations obtained from Doppler data are in error. Figure 6 gives an extreme example of this type of error. As a result, the telemeter data was used as a guide in fairing the curves of drag coefficient against Mach number at transonic speeds.

Based on comparisons of the telemetered and Doppler drag-coefficient data for all models and the error in air velocity, the probable errors of the faired curves of total-configuration drag coefficient against Mach number are as follows:

Total drag coefficient. ± 0.0007
 Mach number ± 0.01

The errors in the results due to any rocket-motor afterburning are not included in these values. Rocket-motor afterburning affects the drag through changes in base pressure. Since base drag has been measured in these tests and can be subtracted from the total drag, errors due to rocket-motor afterburning can be eliminated. In these tests the base drag was always small, and as a result, any affects of rocket-motor afterburning would not materially alter the total drag coefficients. However, the previously listed errors apply to the measured drag or the fore drag obtained by subtracting base drag from total drag. The errors in the measured base pressure coefficients are estimated to be as follows:

M	Errors
1.3	± 0.01
1.0	± 0.02
.9	± 0.03

The Reynolds number range of each flight, based on the mean aerodynamic chord of the wing for the winged models and on body length for the wingless models, is shown as a function of Mach number in figure 7.

RESULTS AND DISCUSSION

Drag

Basic data.- In figure 8 are presented the basic data: total drag coefficient against Mach number for each model and the base drag and base pressure coefficient against Mach number for each model except models 7 and 10. The data for models 4, 5, and 8 presented in the references (indicated in table I) differ especially at transonic speeds from the data in this report, since the wind corrections for these models were large. No wind corrections were made to the previously reported data. Figure 9 presents the data obtained when the vehicle shown in figure 3 was flown for the purpose of determining the drag of the two-fin and four-fin stabilizing arrangements.

Normal-force coefficient against Mach number is presented in figure 10 for the model with the large 6-percent-thick delta wing (model 5). The data substantiate the assumption that the models of the present tests were flown at very near zero lift.

The determination of wing-plus-interference drag coefficient is illustrated in figure 11 for one of the winged configurations of the present tests (model 6). The fin and base drag coefficients of the winged and wingless models were subtracted algebraically from their respective total drag coefficients. The difference between the two resulting values is the wing-plus-interference drag coefficient. In this manner the wing-plus-interference drag was determined for each of the winged models. The accuracy of the wing-plus-interference drag coefficient at transonic speeds is determined mainly by the accuracy of the Mach numbers for the winged and wingless models.

Comparison of straight, swept, and delta wings.- The zero-lift drag coefficients of models with straight (model 12), delta (model 3), and swept (models 6, 9, and 10) wings having equal areas and similar round-nose airfoil sections are shown in figure 12(a), and the corresponding wing-plus-interference drag coefficients are shown in figure 12(b). These wings are of practical interest. A comparison of the drag of the straight-wing model with the drags of the delta- and swept-wing models 3, 6, and 9 reveals the large reduction of transonic drag obtained from moderate and high leading-edge sweep at thickness ratios below 6 percent. However, at low supersonic speeds the drag of model 6, with moderate wing sweepback, was approximately equal to that of the straight-wing model. The delta-wing model and the swept-wing model 9 had comparatively low transonic and supersonic drag. The drag-saving combination of high sweep and small thickness of the delta-wing model is apparent at supersonic speeds; however, at transonic speeds the swept-wing model 9, with greater thickness than the delta-wing model, had lower drag. The drag of swept-wing model 10 was, comparatively speaking, extremely high at

transonic speeds; however, its drag-rise Mach number of approximately 0.94 compared favorably with that of the other models. Generally, as shown in figure 12(b), an increase in the angle of sweepback caused a corresponding decrease in the peak of the drag rise. The one exception was model 10, which had a thick, sweptback wing of high aspect ratio; for this wing the penalty imposed by thickness offset the favorable drag effect associated with a sweptback wing.

The drag "buckets" which occur in most of the curves near the drag-rise Mach number are believed to be real, although they are not clearly understood. The pressure drag over the boattail of the model of reference 9 showed a similar effect.

Effect of changing section of straight wings.- Two straight-wing models (2 and 12) which differed only in shape of the airfoil sections are compared in figure 13. Figure 13(a) shows a comparison of the total-configuration drag coefficient and figure 13(b) gives a comparison of wing-plus-interference drag coefficient. The model having the NACA 65A004.5 section (model 12) had much less drag at transonic speeds than did the model having a sharp-leading-edge section. At supersonic speeds the round-leading-edge model had an approximately constant drag coefficient, whereas the drag coefficient of the sharp-leading-edge model continually decreased at supersonic speeds. (It cannot be said that the round nose of the 65A004.5 airfoil caused the reduction in drag, since the rear portion of this airfoil had a lower slope than that of the hexagonal section.) Model 2 experienced initial drag rise at $M = 0.82$; this low value may have been due to the breaks in the contour of the airfoil section.

Effect of increasing thickness of delta wings.- A comparison of the drag coefficients of the two large delta wings and a modified delta wing having 3-, 6-, and 4.5-percent thickness, respectively, is shown in figure 14.

Within the accuracy of the data there appears to be no effect of wing thickness on the drag-rise Mach number for these wings. The primary difference in level of the curves is the result of varying the thickness.

It is interesting to note that the wing-plus-interference drag of the 6-percent-thick delta wing is of the same magnitude as the total drag of the 3-percent-thick delta-wing model. The total volume of the 3-percent-thick delta-wing model was approximately twice that of the exposed 6-percent-thick delta wing. Thus, on the basis of these tests, it appears that for minimum zero-lift drag it is more profitable to add volume to a body than to increase the wing thickness ratio if larger configuration volume is desired.

Effect of body size.- The drag coefficients of models with small and large 3-percent-thick delta wings are compared in figure 15. These

results show that, for these configurations, the difference in wing-body interference drag is small.

Effect of body shape.- A comparison of the drag coefficients of the swept wing on the parabolic body (model 6) and on the transonic body (model 7) is shown in figure 16.

No base pressure values were obtained for the transonic model 7. As a result, no correction for the base drag interference was made; however, on all other models the base drag interference was small, so that neglect of this correction should not change the results noticeably. These results show that the configuration having its wing behind the maximum diameter of the body and the smallest curvature of the afterbody (model 6) had less wing-plus-interference drag at transonic speeds. Recently obtained unpublished data from the Langley 8-foot transonic tunnel show the same trends.

Above a Mach number of approximately 1.2 the body configuration apparently had little effect on the interference drag. These results, together with those shown in figure 15, indicate that differences in the shape and size of the body relative to the wing can have a large effect on the interference drag of a wing-body configuration at transonic speeds but is of much less significance at higher and lower speeds.

Effects of surface finish.- The drag coefficients of two swept-wing models and two wingless models which were identical except for the surface finish are compared in figure 17. The fore drag coefficient of each model, obtained by subtracting base drag coefficient from total drag coefficient, is presented in figure 17(a) in order to separate from the data any effects of surface finish or rocket-motor afterburning on base drag. Wing-plus-interference drag coefficients are presented in figure 17(b) and base pressure coefficients are presented in figure 17(c). As shown in figure 17(a), the configurations with the nonglossy finish had higher drags at subsonic and low supersonic speeds. At higher speeds the differences in drag were small and within the accuracy of the data. The wing-plus-interference drags were not greatly affected by the difference in surface finish. The major difference in drag apparently occurs on the bodies of the configurations. As shown in figure 17(c), the base pressure coefficients were not affected by the differences in finish. The large differences in pressure coefficient are probably the result of intermittent rocket-motor afterburning.

In figure 18 is presented a comparison of the drag coefficients of two wingless models (11 and 11(a)), identical except for surface finish. Model 11(a) was finished with orange lacquer, which recent tests have shown to deteriorate (because of surface temperature) at Mach numbers above 1.5. Model 11 was finished with clear lacquer, which remains good

to a Mach number of 1.75. The maximum Mach number reached by model 11(a) was about 2.0, whereas that reached by model 11 and all other models was less than 1.75. It is believed that the 20-percent increase in drag of model 11(a) was caused by increased roughness resulting from deterioration of the orange-lacquer finish. Because of this, the wing-plus-interference drag for model 7 presented in references 4 and 5 is in error. Since the publication of references 4 and 5, an additional correction has been made to the data to correct for flight-path curvature. As a result, the total-configuration drag coefficients for models 7 and 11a presented in references 4 and 5 are also in error.

Base Pressures

In figure 19 are presented base pressure coefficients against Mach number for models 1, 2, 3, 4, 5, 6, and 12. The magnitude of the base pressures measured indicates that the bases contributed less than 4 percent of the total drag of the test models. The irregularities in base pressure may be the result of rocket-motor afterburning. Generally, the base pressures for the winged models are greater (less drag) than for the wingless configuration. It appears that base pressure is affected by the size and shape of the wings mounted on the body. The base pressures for all the winged models peak at Mach numbers near 0.975. The base pressure peak for the wingless model occurs at $M = 0.99$. This agrees with the results for similar bodies presented in reference 10.

Maximum Lift-Drag Ratios

The foregoing zero-lift drag results are of particular interest in relation to the performance of aircraft designed to operate at low lift coefficients. For aircraft designed to operate at higher lift coefficients for greater efficiency, however, the maximum ratio of lift to drag is of particular interest. Accordingly, the present configurations are examined in this light and the results are shown in figure 20 as the variation of maximum lift-drag ratio with Mach number for each of the tested configurations. The maximum lift-drag ratios were determined from the relationship

$$(L/D)_{\max} = \frac{1}{2} \sqrt{\frac{1}{(dC_D/dC_L^2) C_D}}$$

This relationship assumes that dC_D/dC_L^2 remains linear up to the C_L for $(L/D)_{\max}$.

~~CONFIDENTIAL~~

Values of C_D were obtained from the present results. The values of the drag parameter dC_D/dC_L^2 were obtained from other rocket-model tests for wings similar to those of the present tests but in the presence of a different basic body which had a horizontal tail. Parameters for the present wings were obtained by rocket-model flights from the following sources: the straight wing (model 2) from reference 11; the swept wings (models 5 and 6) and the delta wings (models 3, 4, and 5) from unpublished data; the modified delta wing (model 8) from reference 6; and the swept wing (model 9) from reference 7. Except for the large thin delta wing (model 4) and the modified delta wing (model 8), the maximum lift-drag ratios of all models were approximately 7.0 at low supersonic speeds. The model with a large thin delta wing had maximum lift-drag ratios of about 8.0 at supersonic speeds as a result of its comparatively low total-configuration drag, as shown in figure 14(a). The modified delta-wing model had maximum lift-drag ratios of from 9 to 9.5 at supersonic speeds as a result of its low zero-lift drag and drag due to lift.

CONCLUSIONS

Ten airplane-like configurations have been flown at Mach numbers from 0.8 to 1.6 and at large Reynolds numbers. The following general statements summarize the results.

1. Of several wing-body configurations having straight, swept, and delta wings of equal area, a 3-percent-thick, 60° delta wing had the least zero-lift drag at supersonic speeds. At transonic speeds, however, a 5.6-percent-thick, 60° swept wing had the least drag. At low supersonic speeds the maximum lift-drag ratios for all models were between 7 and 9.5.
2. Changing the section of otherwise identical straight wings from a hexagonal section to an NACA 65A004.5 section resulted in a 23-percent reduction in zero-lift drag coefficient at transonic speeds.
3. Doubling the thickness of the 3-percent-thick, 60° delta wing added roughly 40 percent to the configuration drag and 60 percent to the wing drag at zero lift.
4. Differences in body profile shape had a large effect on the interference drag of a wing-body combination at transonic speeds, but were of less significance at subsonic and supersonic speeds for the specific bodies studied in this investigation.

5. The base pressures on the bodies of the present configurations indicate base drags of very small magnitude. The pressures were affected by the size and shape of the wings mounted on the body.

Langley Aeronautical Laboratory,
National Advisory Committee for Aeronautics,
Langley Field, Va.

REFERENCES

1. Nelson, Robert L.: Large-Scale Flight Measurements of Zero-Lift Drag at Mach Numbers From 0.86 to 1.5 of a Wing-Body Combination Having a 60° Triangular Wing With NACA 65A003 Sections. NACA RM L50D26, 1950.
2. Schult, Eugene D.: Large-Scale Flight Measurements of Zero-Lift Drag at Mach Numbers From 0.8 to 1.6 of a Wing-Body Combination Having an Unswept 4.5-Percent-Thick Wing With Modified Hexagonal Sections. NACA RM L51A15, 1951.
3. Schult, Eugene D.: Comparison of Large-Scale Flight Measurements of Zero-Lift Drag at Mach Numbers From 0.9 to 1.7 of Two Wing-Body Combinations Having Similar 60° Triangular Wings With NACA 65A003 Sections. NACA RM L50I22, 1950.
4. Langley Pilotless Aircraft Research Division: Some Recent Data From Flight Tests of Rocket-Powered Models. NACA RM L50K24, 1951.
5. Katz, Ellis: Flight Investigation From High Subsonic to Supersonic Speeds To Determine the Zero-Lift Drag of a Transonic Research Vehicle Having Wings of 45° Sweepback, Aspect Ratio 4, Taper Ratio 0.6, and NACA 65A006 Airfoil Sections. NACA RM L9H30, 1949.
6. Chapman, Rowe, Jr., and Morrow, John D.: Longitudinal Stability and Drag Characteristics at Mach Numbers From 0.70 to 1.37 of Rocket-Propelled Models Having a Modified Triangular Wing. NACA RM L52A31, 1952.
7. Vitale, A. James, McFall, John C., Jr., and Morrow, John D.: Longitudinal Stability and Drag Characteristics at Mach Numbers From 0.75 to 1.5 of an Airplane Configuration Having a 60° Swept Wing of Aspect Ratio 2.24 As Obtained From Rocket-Propelled Models. NACA RM L51K06, 1952.
8. Morrow, John D., and Katz, Ellis: Flight Investigation at Mach Numbers From 0.6 to 1.7 To Determine Drag and Base Pressures on a Blunt-Trailing-Edge Airfoil and Drag of Diamond and Circular-Arc Airfoils at Zero Lift. NACA RM L50E19a, 1950.
9. Stoney, William E., Jr.: Pressure Distributions at Mach Numbers From 0.6 to 1.9 Measured in Free Flight on a Parabolic Body of Revolution With Sharply Convergent Afterbody. NACA RM L51L03, 1952.

10. Katz, Ellis R., and Stoney, William E., Jr.: Base Pressures Measure on Several Parabolic-Arc Bodies of Revolution in Free Flight at Mach Numbers From 0.8 to 1.4 and at Large Reynolds Numbers. NACA RM L51F29, 1951.
11. Gillis, Clarence L., and Vitale, A. James: Wing-On and Wing-Off Longitudinal Characteristics of an Airplane Configuration Having a Thin Unswept Tapered Wing of Aspect Ratio 3, As Obtained From Rocket-Propelled Models at Mach Numbers From 0.8 to 1.4. NACA RM L50K16, 1951.

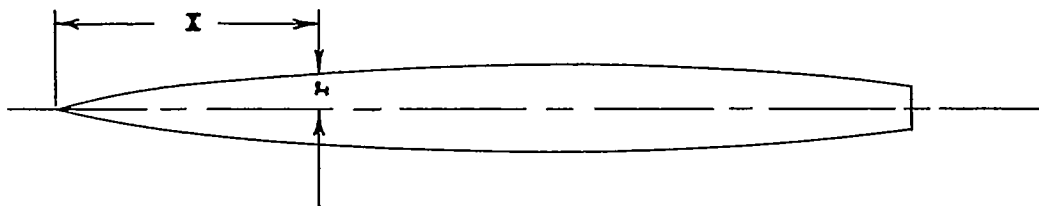
TABLE I.- CONFIGURATIONS OF THE INVESTIGATION

Model	Body shape	Wing								
		Designation	Λ (deg)	A	λ	Airfoil	S_f/S_w	M.A.C.	S_w/S_e	Reference
1, 1a	Parabolic	Wingless								^a 1, 2
2	Parabolic	Straight	0 at 0.75c	3.04	0.394	Hexagonal; $\frac{t}{c} = 0.045$	0.0606	2.375	1.25	2, 4
3	Parabolic	Delta	60 at L.E.	2.31	0	NACA 65A003	.0609	3.42	1.40	3, 4
4	Parabolic	Delta	60 at L.E.	2.31	0	NACA 65A003	.0305	4.84	1.261	1, 4
5	Parabolic	Delta	60 at L.E.	2.31	0	NACA 65A006	.0305	4.84	1.261	4
6, 6a	Parabolic	Swept	45 at 0.25c	4.0	.6	NACA 65A006	.0606	1.99	1.191	^b 4
7	Transonic	Swept	45 at 0.25c	4.0	.6	NACA 65A006	.0606	1.99	1.191	4, 5
8	Parabolic	Modified delta	57 at L.E.	2.53	.1	$\frac{t}{c} \begin{cases} \text{root} & .037 \\ \text{tip} & .060 \\ \text{rms} & .0392 \end{cases}$.0305	4.24	1.222	6
9	Parabolic	Swept	63 at L.E.	2.24	.4	^d NACA 64A011 at root NACA 64A008 at tip (both perpendicular to 32.66-percent chord) Free stream $(t/c)_{rms} = 0.0564$.0606	2.85	1.308	7
10	Transonic	Swept	45 at 0.25c	8.0	.45	NACA 63 ₁ A012	.0606	1.44	1.145	
11, 11a	Transonic	Wingless								^c 5
12	Parabolic	Straight	0 at 0.75c	3.04	.394	NACA 65A004.5	.0606	2.375	1.25	

^aModel 1a only.^bModel 6 only.^cModel 11a only.^dFor more complete description of wing see reference.

TABLE II.- BODY COORDINATES FOR TEST MODELS

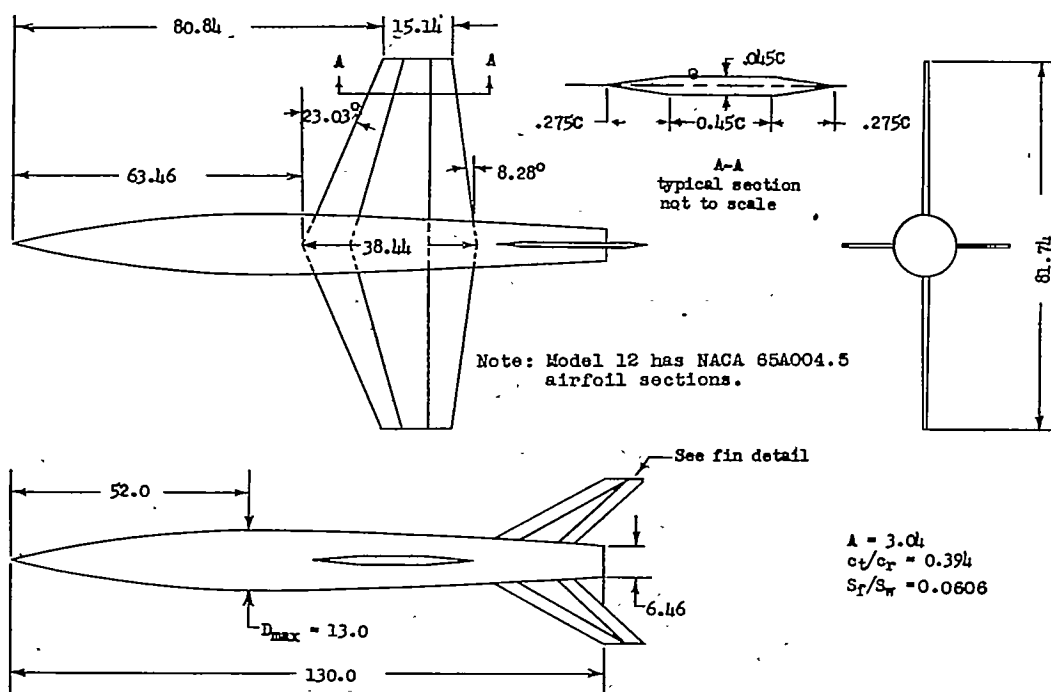
Body coordinates 130-inch parabolic model (in.)			
X	r	X	r
0	0	54.60	6.496
0.78	0.194	62.40	6.442
1.17	.289	70.20	6.322
1.95	.478	78.00	6.137
3.90	.938	85.80	5.886
7.80	1.804	93.60	5.570
11.70	2.596	101.40	5.188
15.60	3.315	109.20	4.742
23.40	4.534	117.00	4.229
31.20	5.460	124.80	3.652
39.00	6.094	130.00	3.230
46.80	6.435		



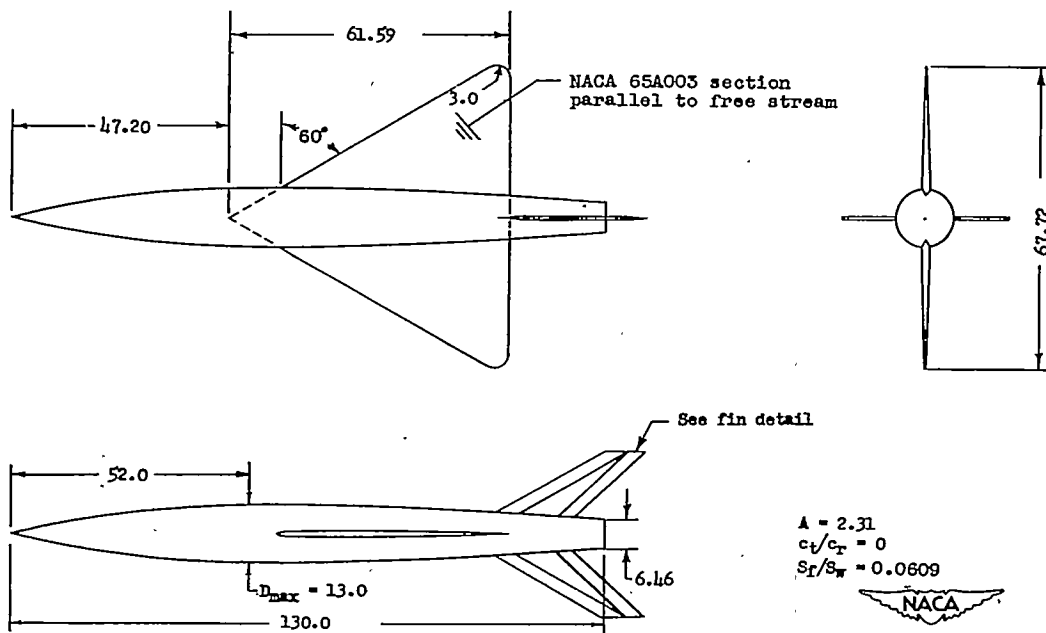
Body coordinates 130-inch transonic model (in.)			
X	r	X	r
0.000	0.000	54.600	6.135
0.780	0.360	62.400	6.339
1.170	0.465	70.200	6.462
1.950	0.668	78.000	6.500
3.900	1.126	85.800	6.442
7.800	1.880	93.600	6.276
11.700	2.517	101.400	5.993
15.600	3.075	109.200	5.556
23.400	4.046	117.000	4.880
31.200	4.820	124.800	3.940
39.000	5.405	130.000	3.231
46.800	5.836		

Nose radius = 0.078 inch



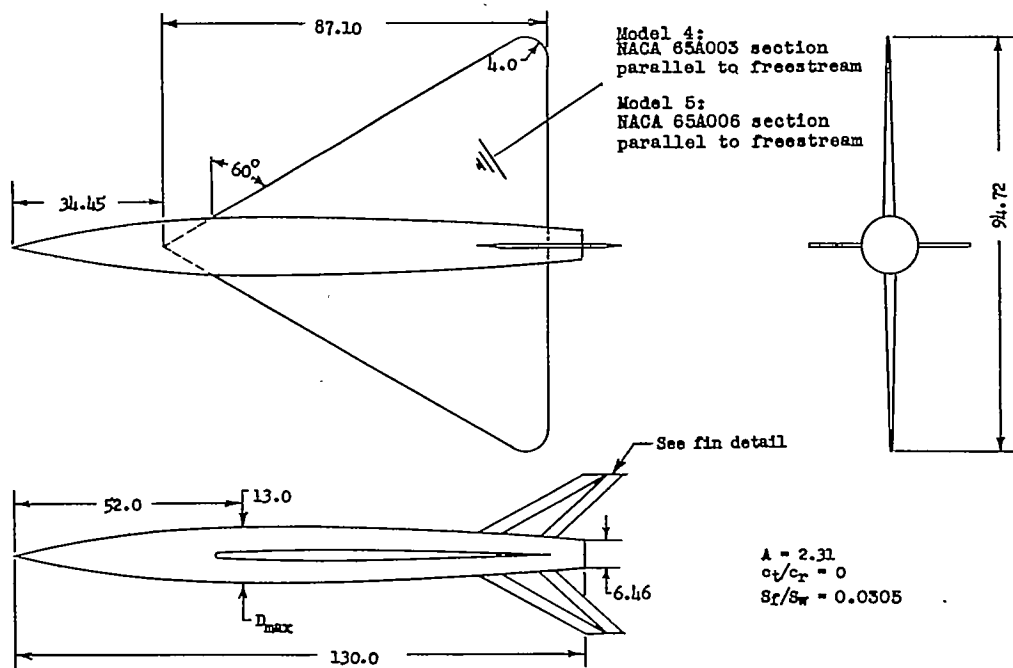


(a) Straight wing (models 2 and 12).

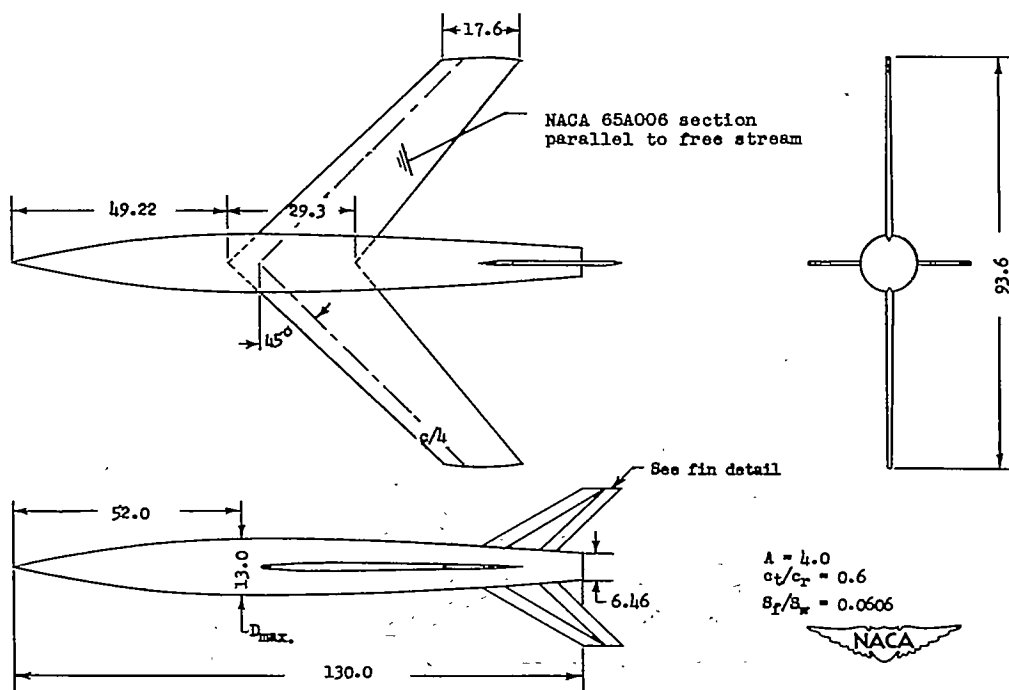


(b) Small 3-percent-thick delta wing (model 3).

Figure 1.- General arrangement of test models. All dimensions are in inches. Wingless models are not shown.

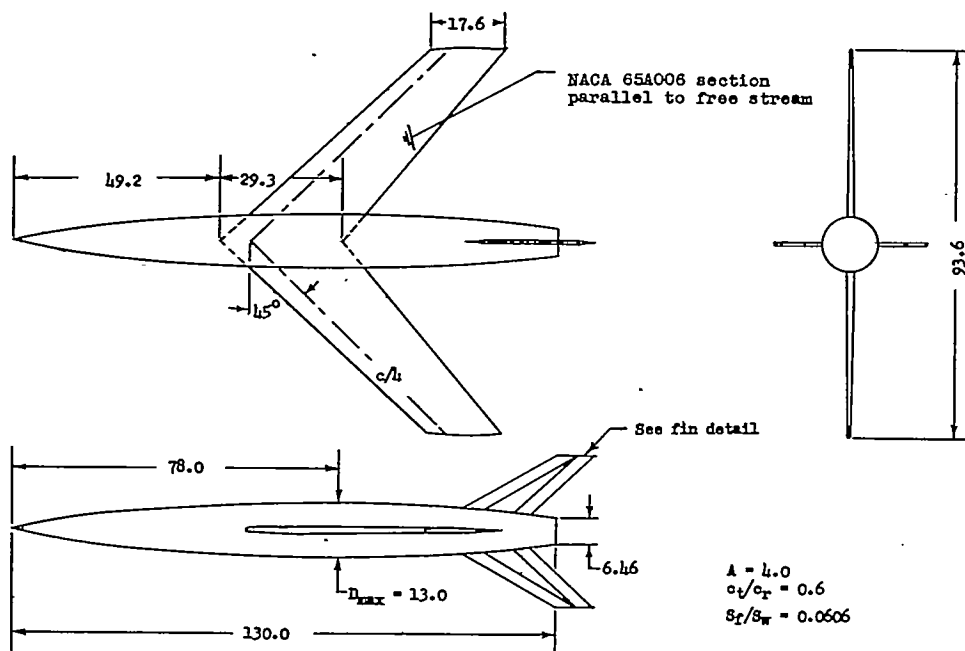


(c) Large 3-percent- and 6-percent-thick delta wings (models 4 and 5).

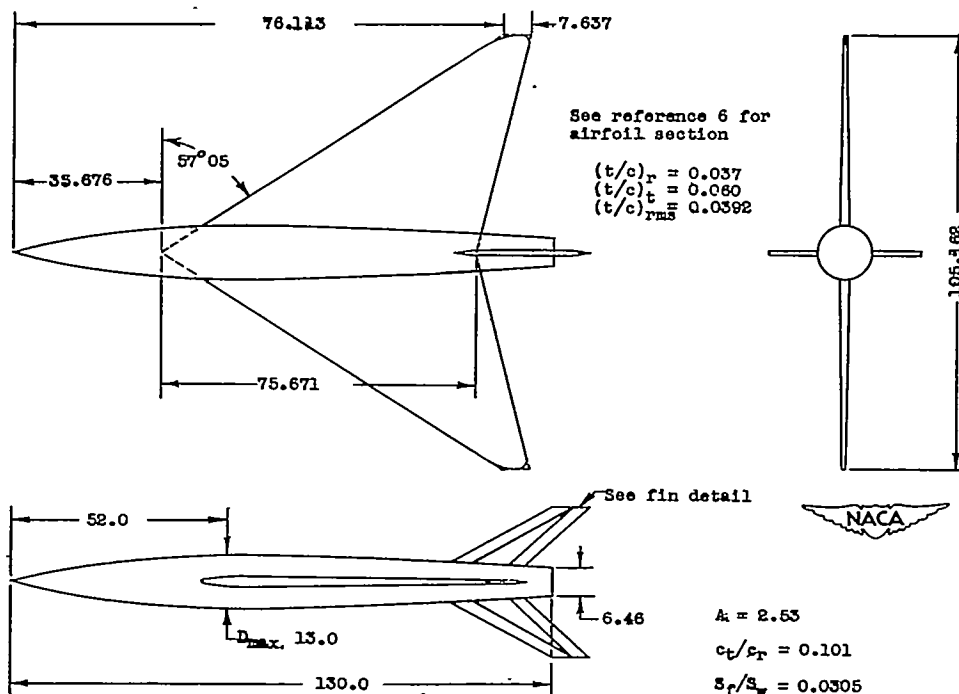


(d) Swept wing on parabolic body (models 6 and 6a).

Figure 1.- Continued.

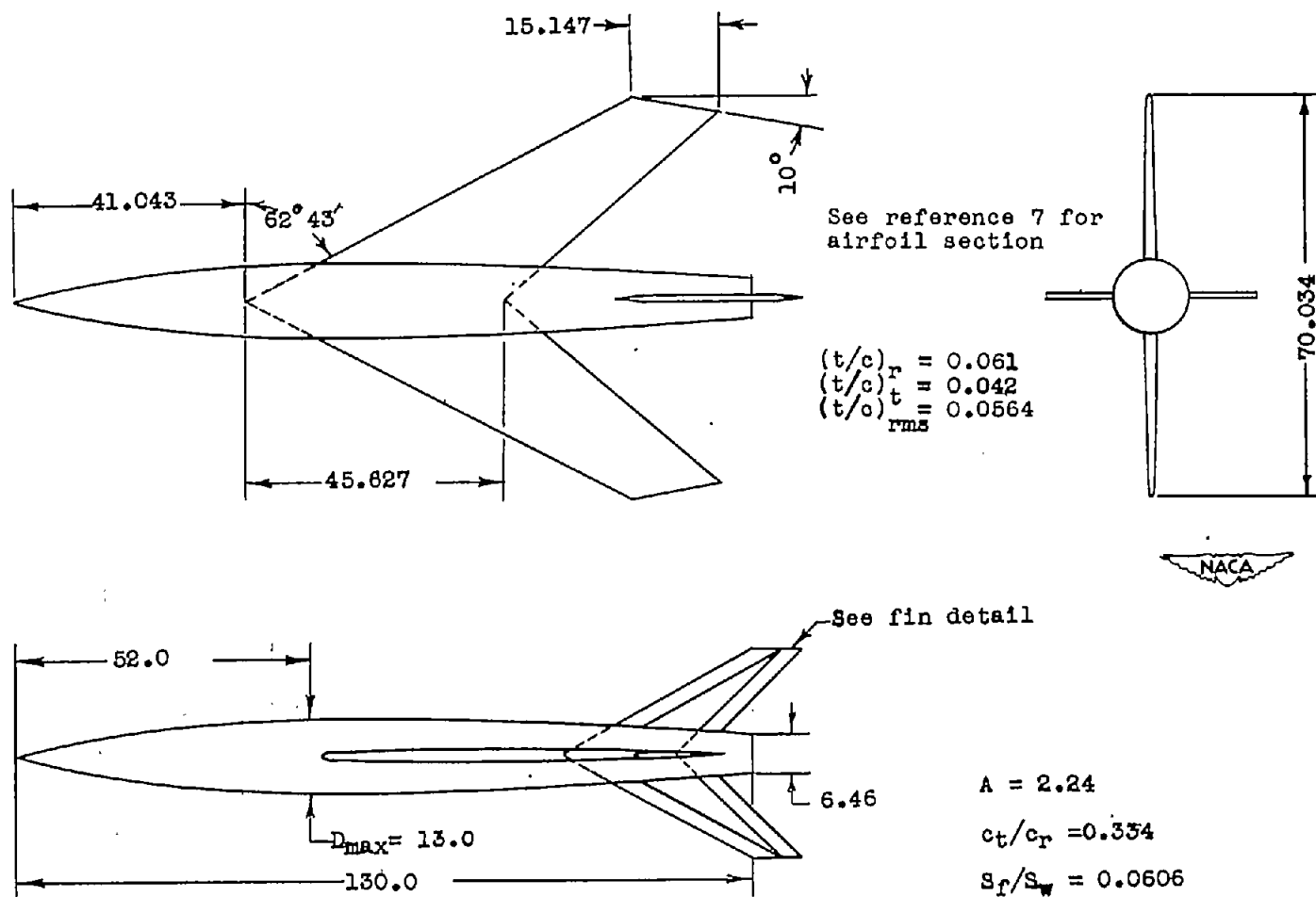


(e) Swept wing on transonic body (model 7).



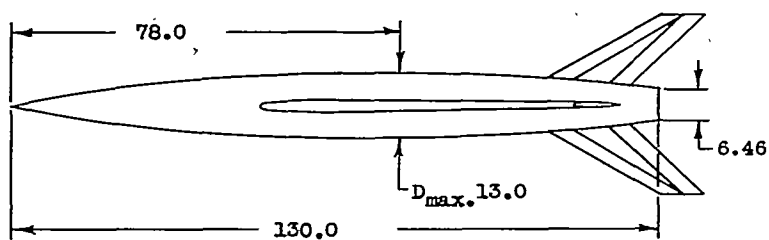
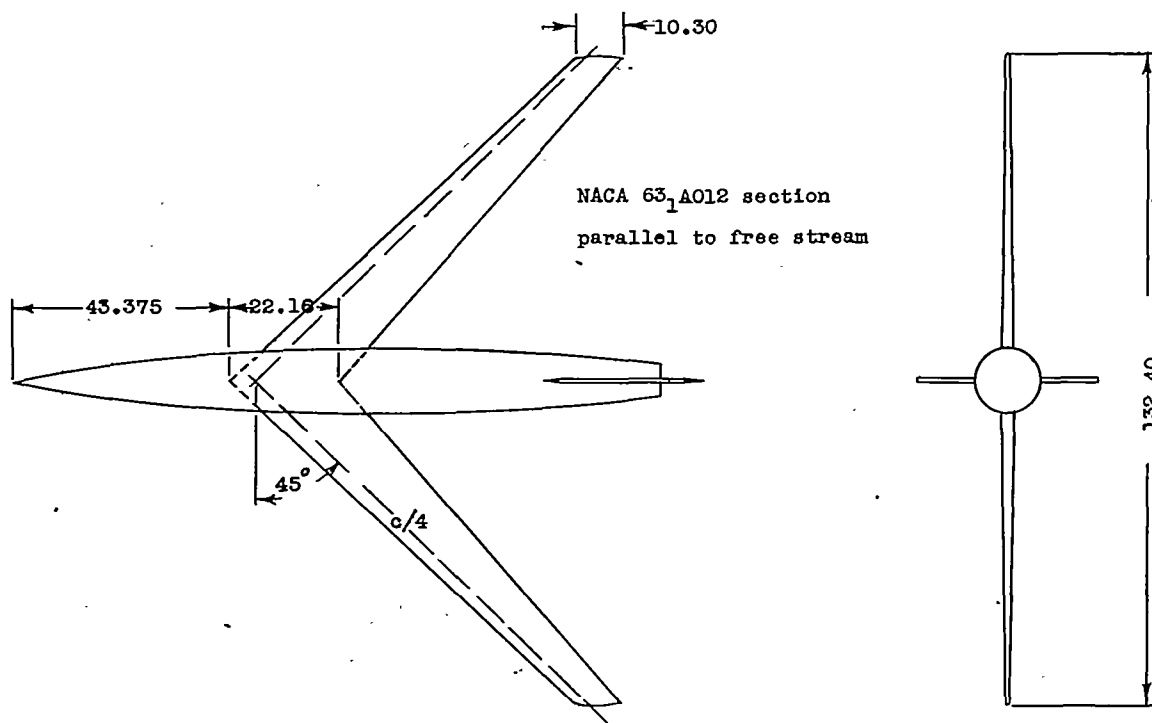
(f) Modified delta wing on parabolic body (model 8).

Figure 1.- Continued.



(g) Swept wing of low aspect ratio on parabolic body (model 9).

Figure 1.- Continued.



$$A = 8.0$$

$$c_{y/c_r} = 0.45$$

$$S_f/S_w = 0.0606$$

(h) Swept wing of high aspect ratio on transonic body (model 10).

Figure 1.- Concluded.

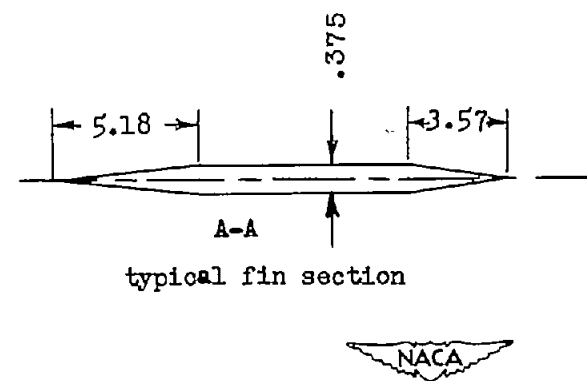
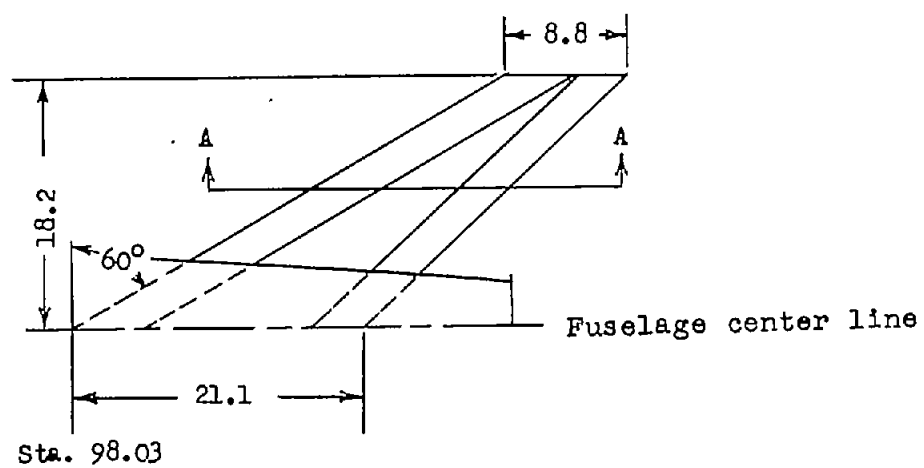


Figure 2.- Detail of typical stabilizing fin. All dimensions are in inches.

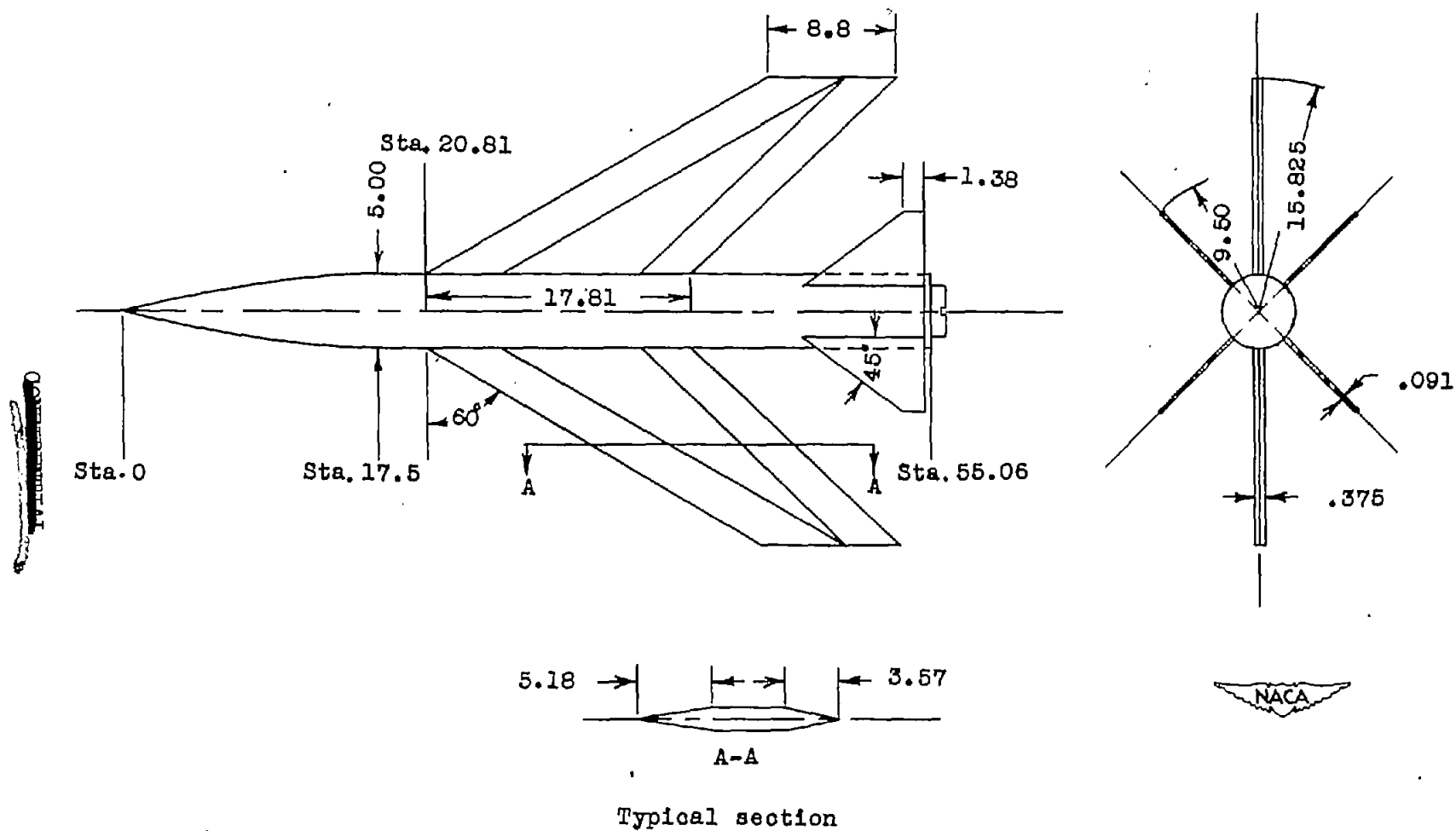


Figure 3.- General arrangement of vehicle used for determining fin drag. Shown with two fins as wings, but was also flown with four fins as wings. All dimensions are in inches.



Figure 4.- General view of a typical model on the launching stand.

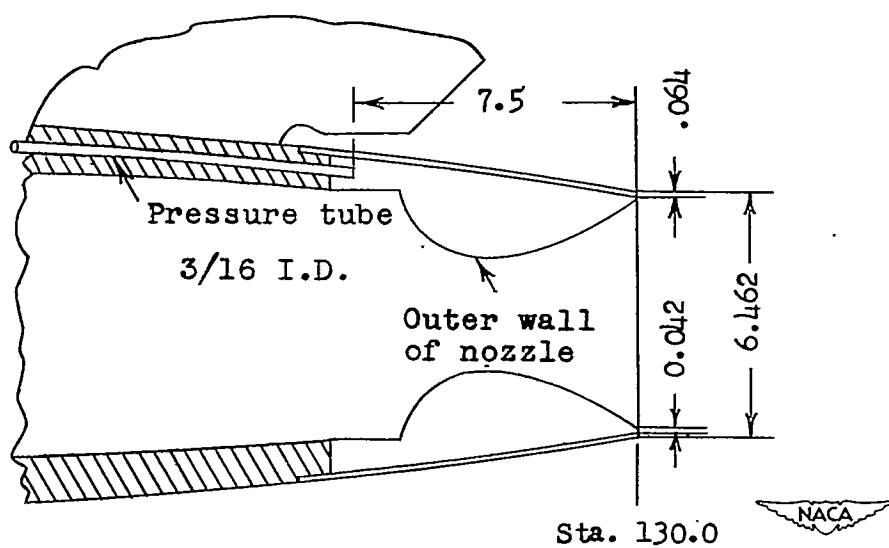


Figure 5.- Detail of base-pressure orifice. All dimensions are in inches.

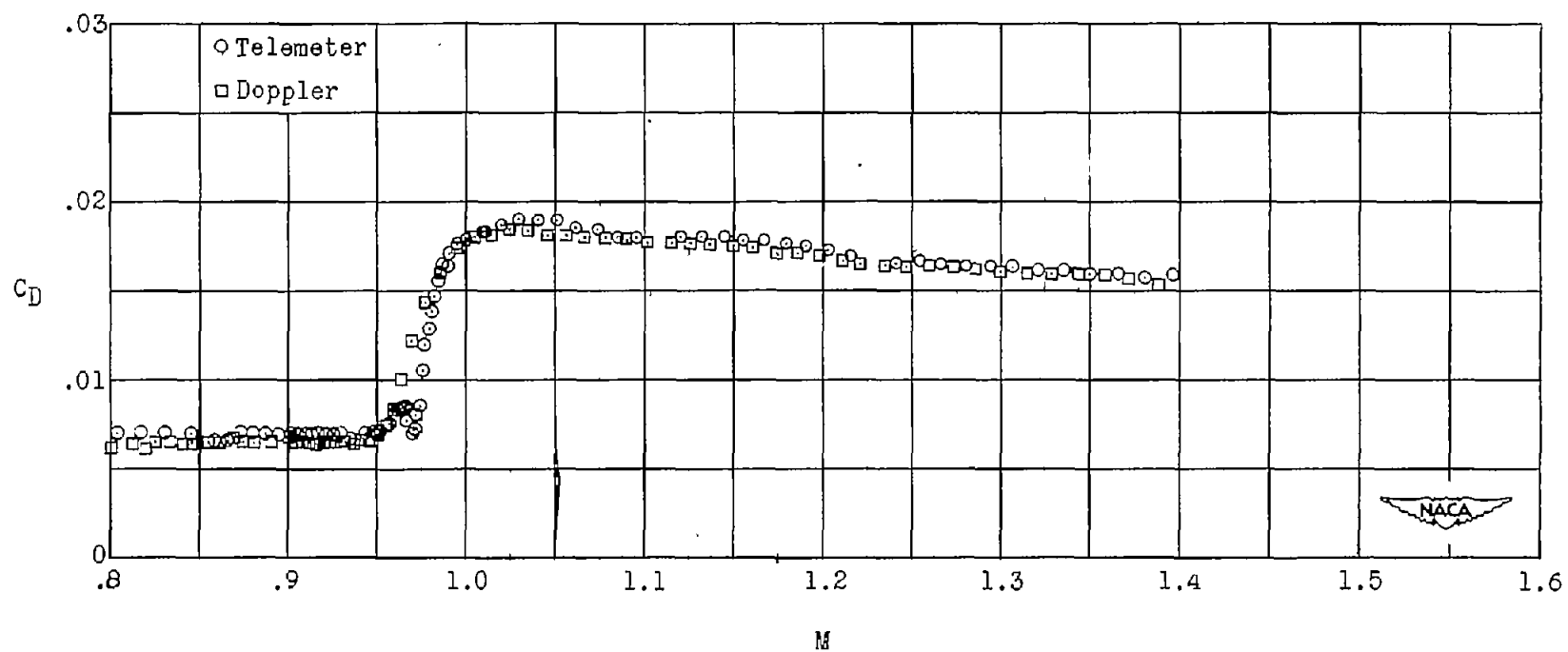


Figure 6.- Basic drag data for a typical configuration (model 5).

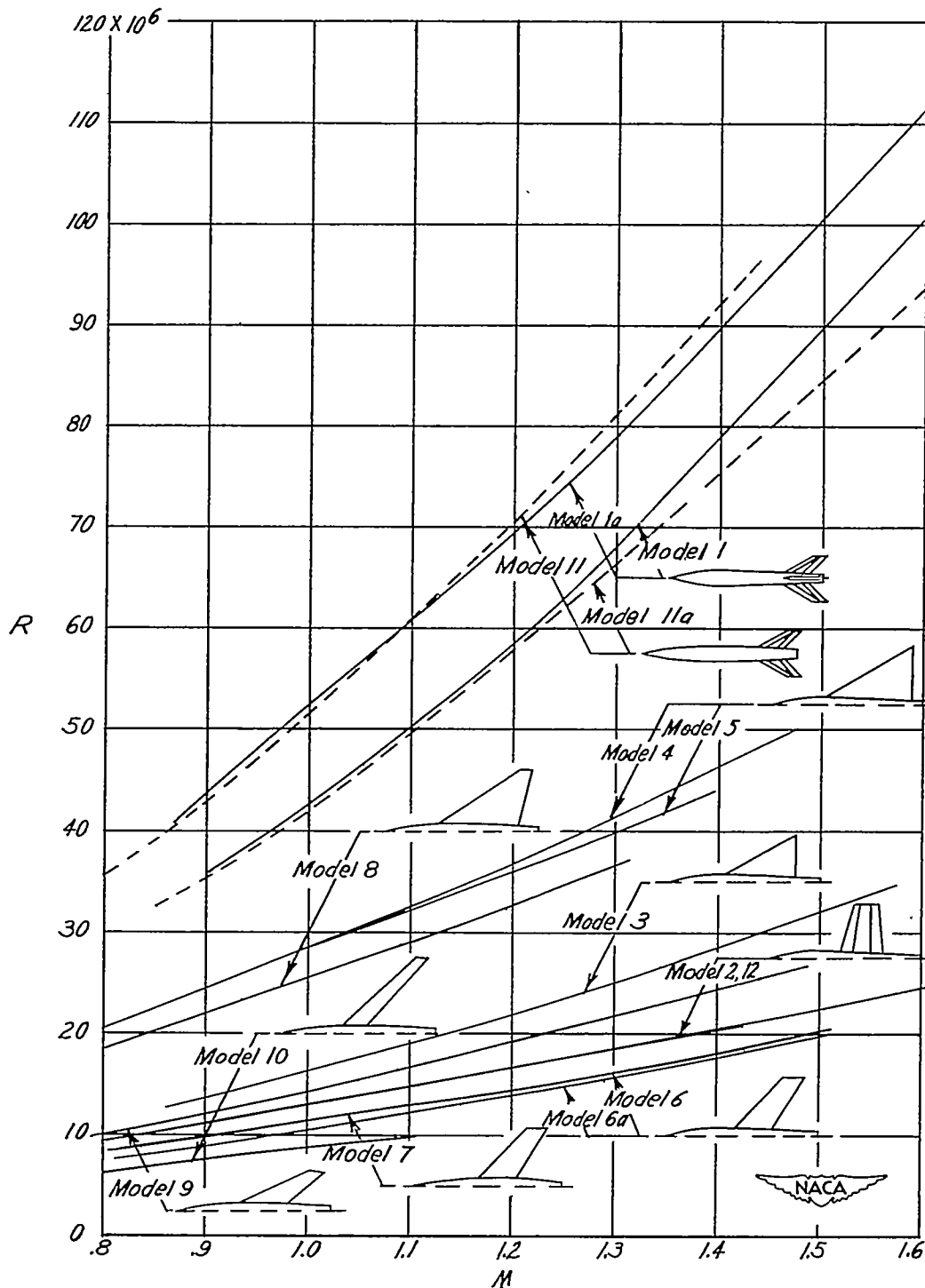
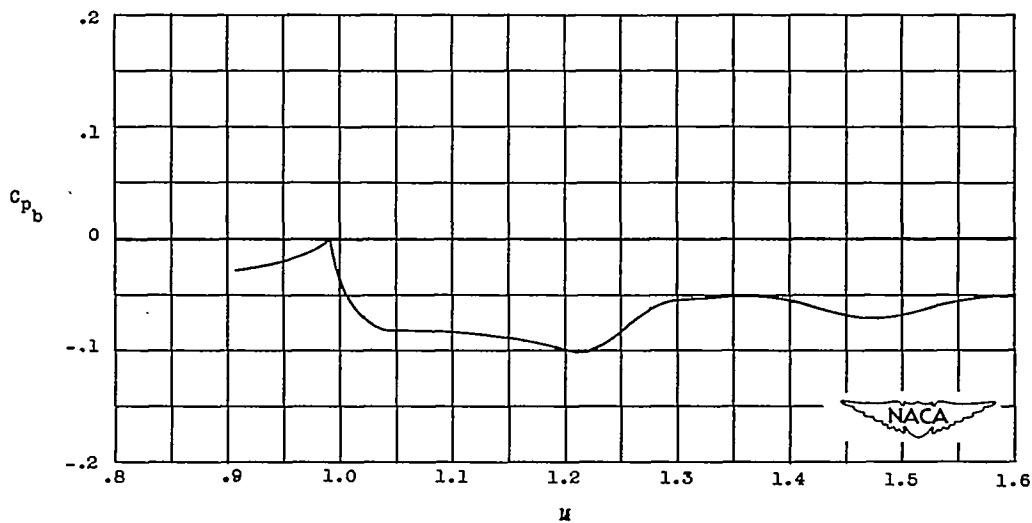
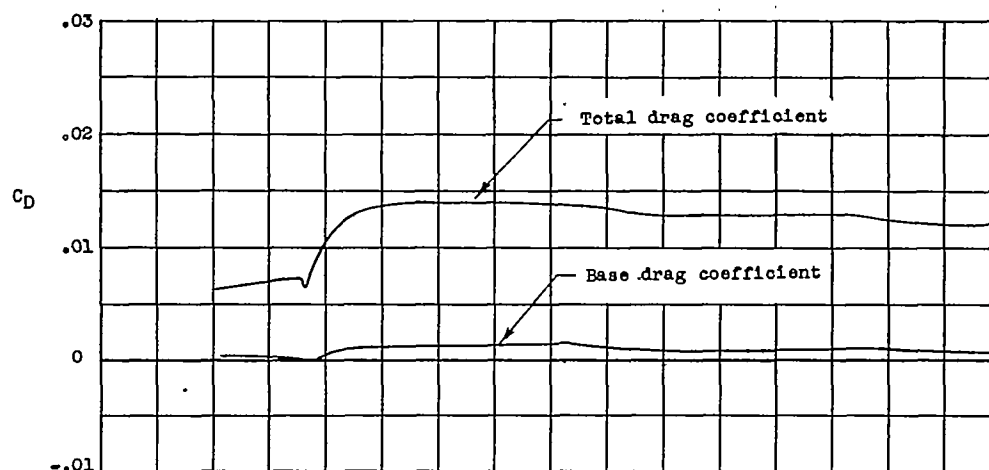
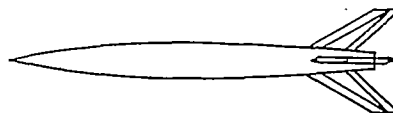


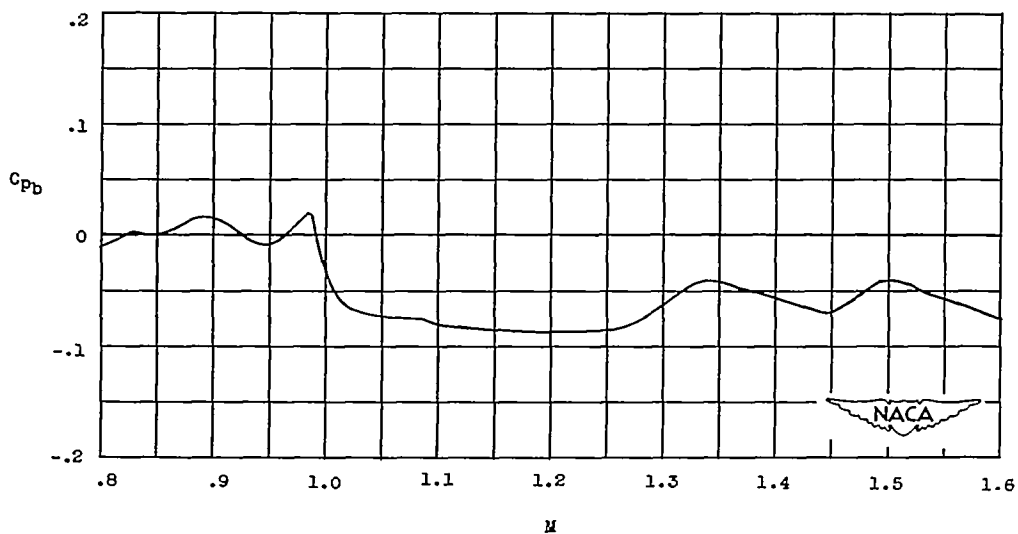
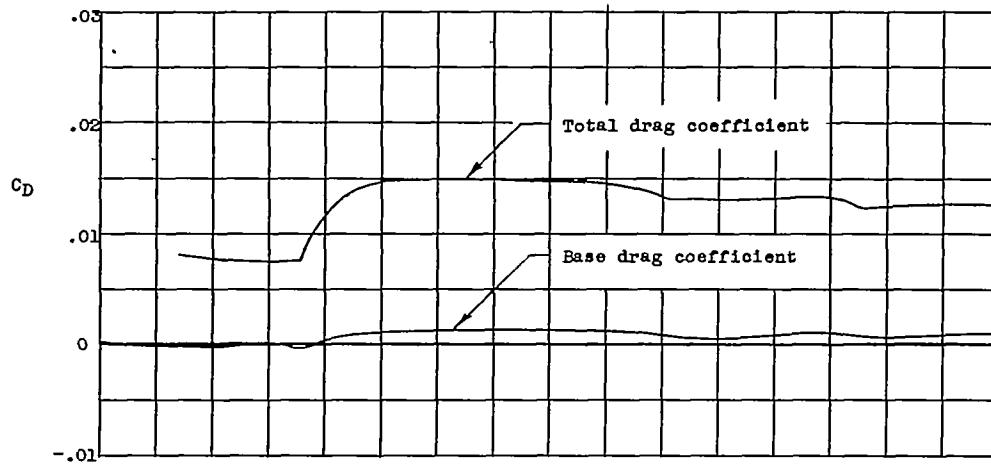
Figure 7.- Comparison of Reynolds numbers for test models. Reynolds numbers for wingless models were based on body length of 10.83 feet and those for winged models were based on their respective mean aerodynamic chords.

CONFIDENTIAL



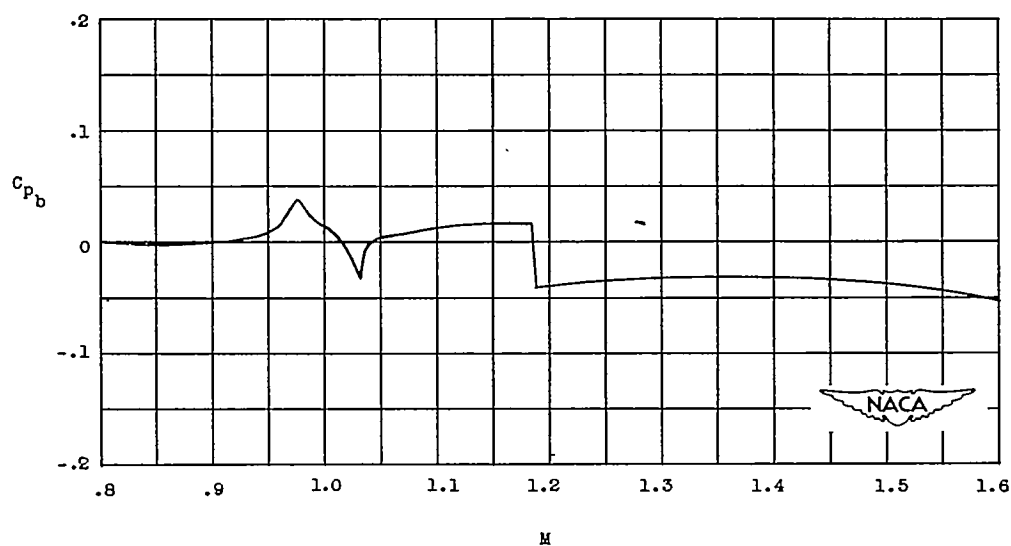
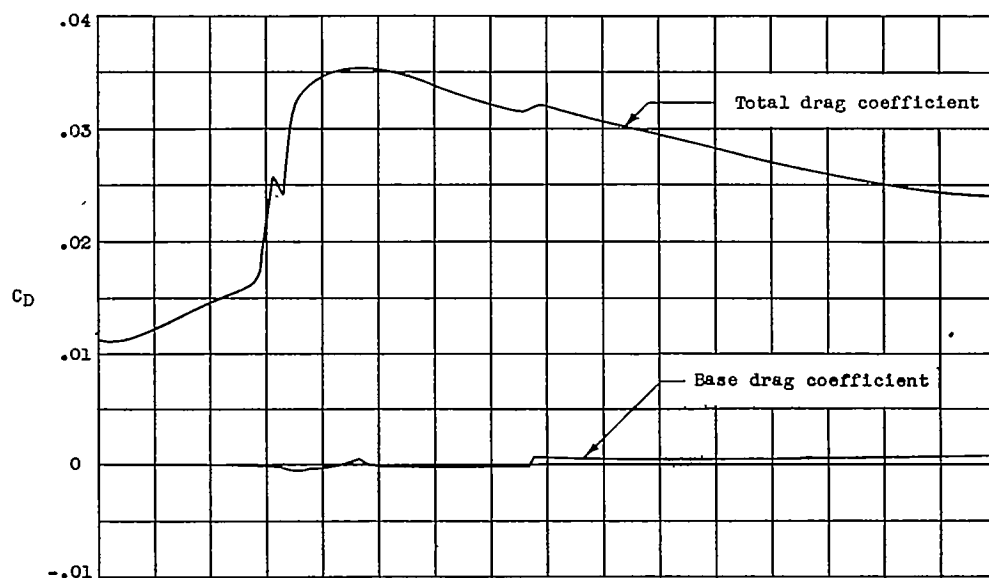
(a) Model 1 (reference 2).

Figure 8.- Test data obtained for each model.



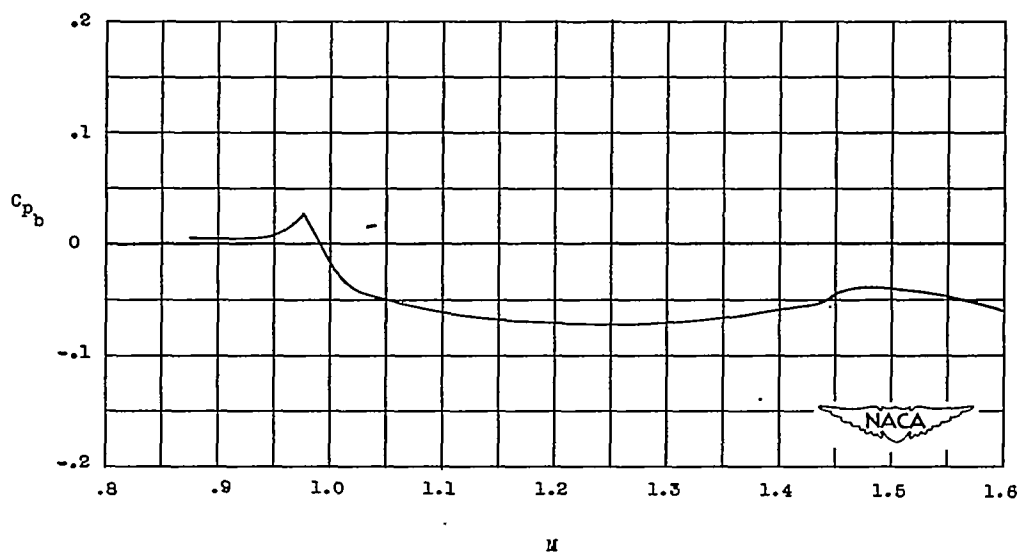
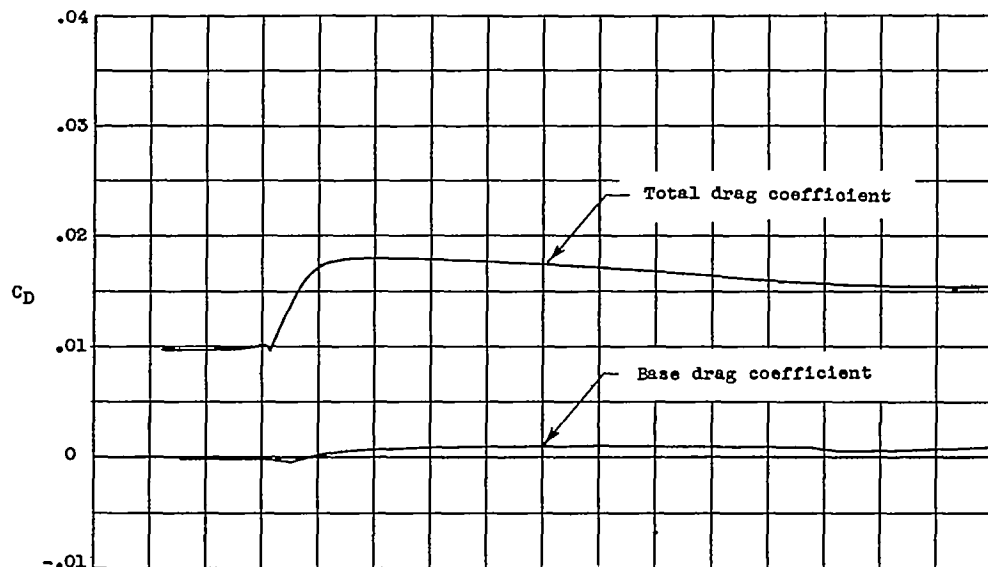
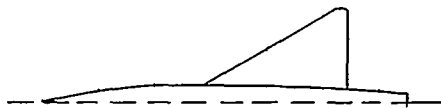
(b) Model 1a (reference 1).

Figure 8.- Continued.



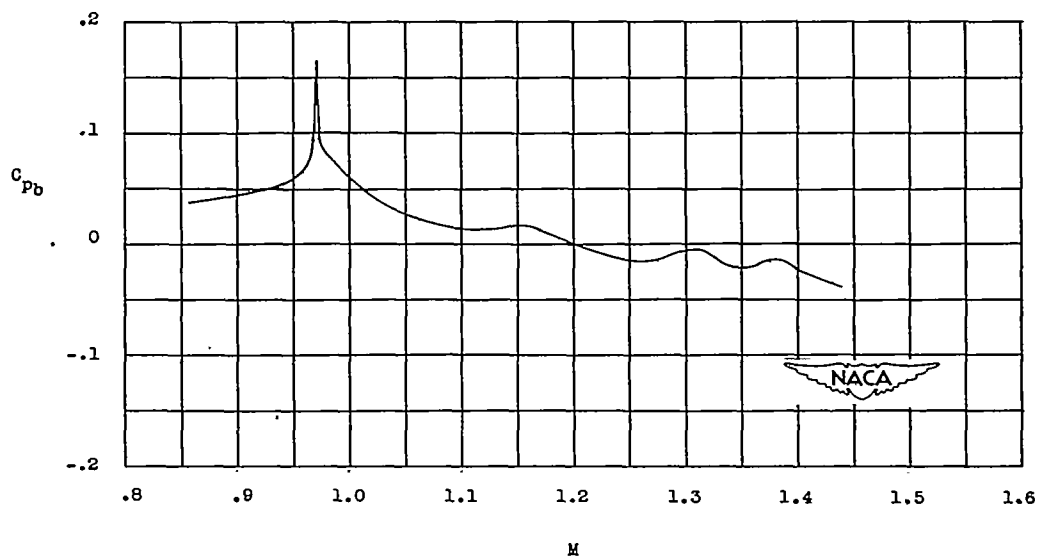
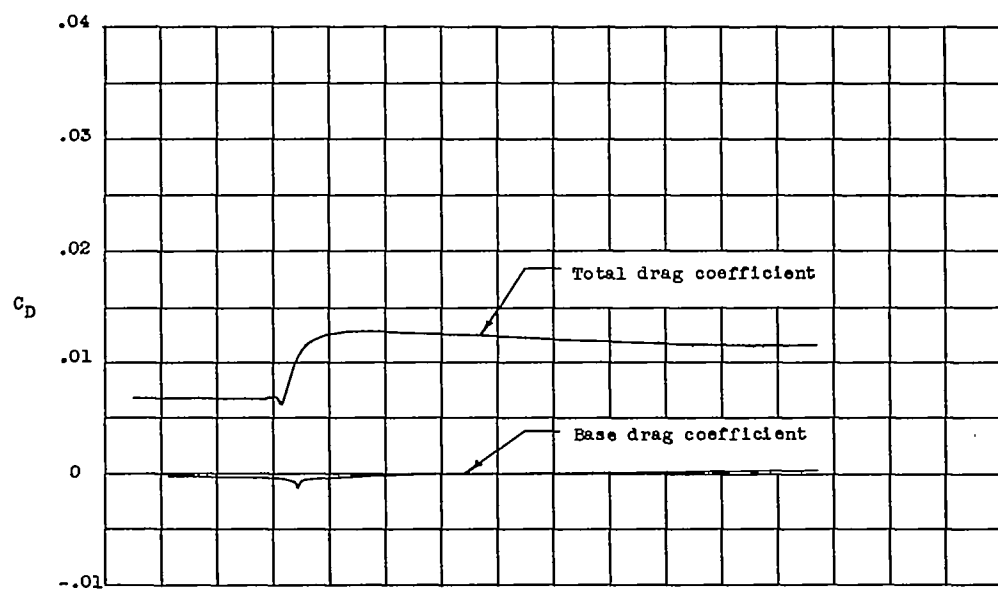
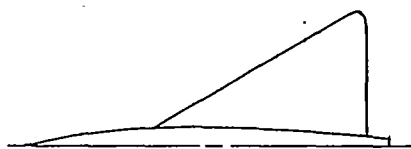
(c) Model 2 (reference 2).

Figure 8.- Continued.



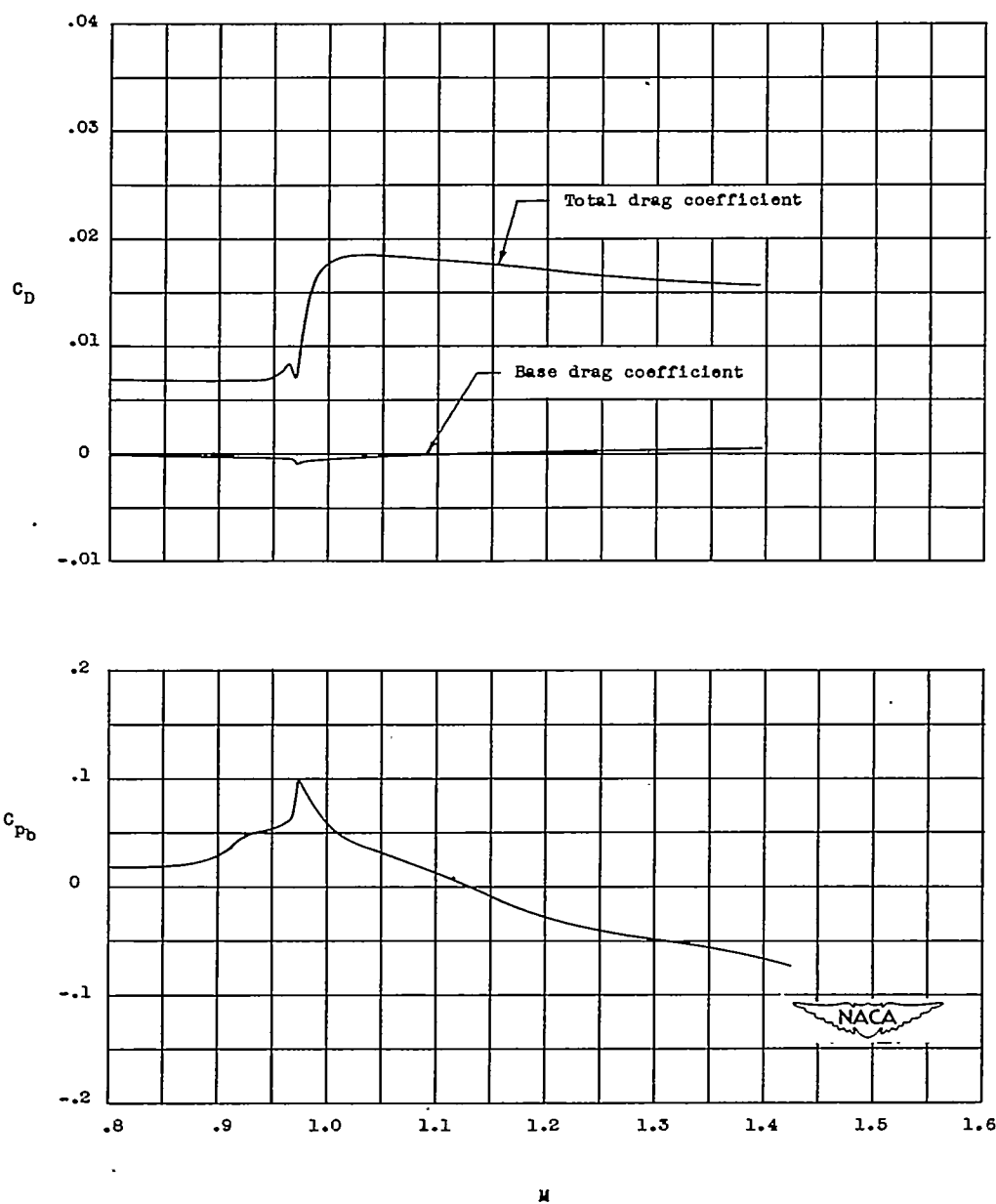
(d) Model 3 (reference 3).

Figure 8.- Continued.



(e) Model 4 (reference 1).

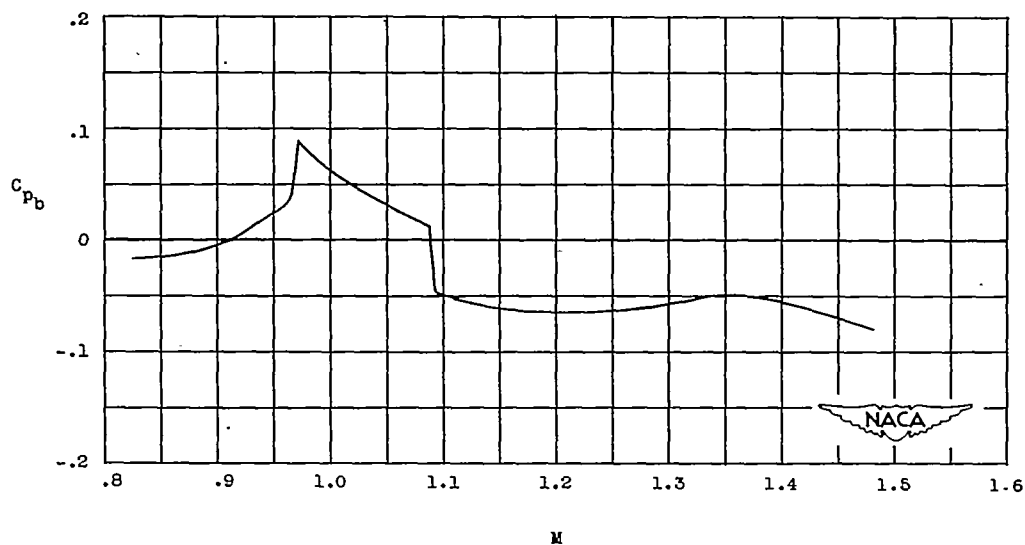
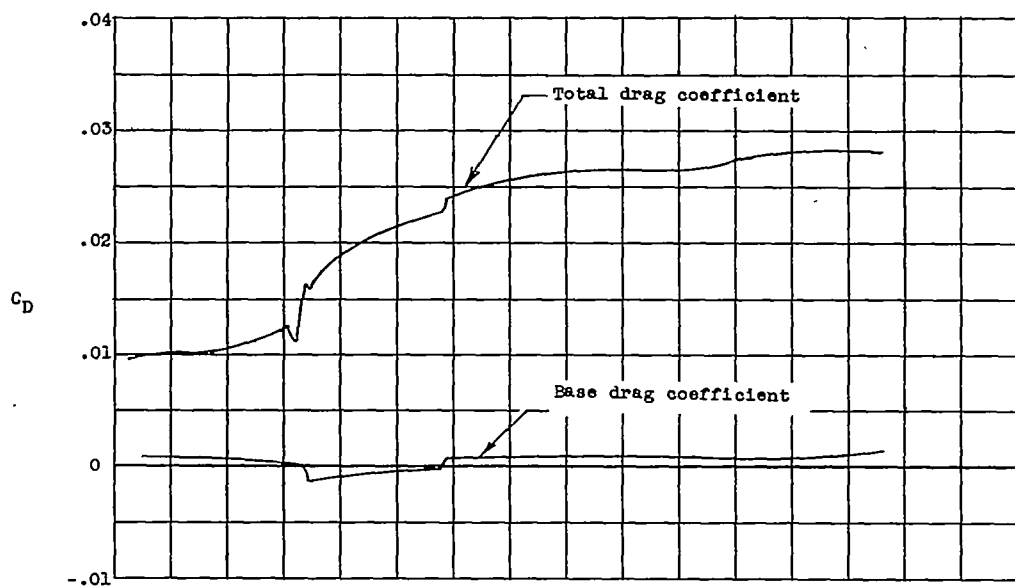
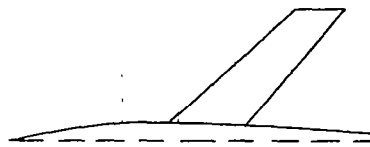
Figure 8.- Continued.

~~CONFIDENTIAL~~

(f) Model 5.

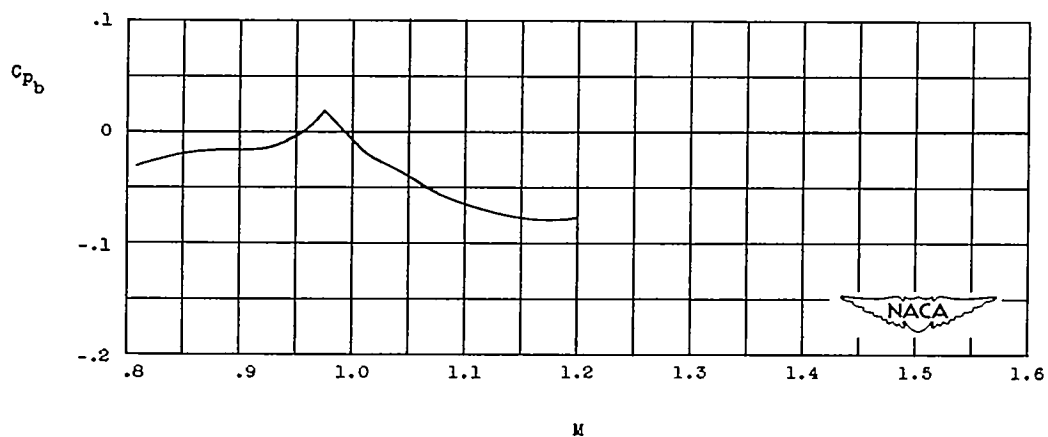
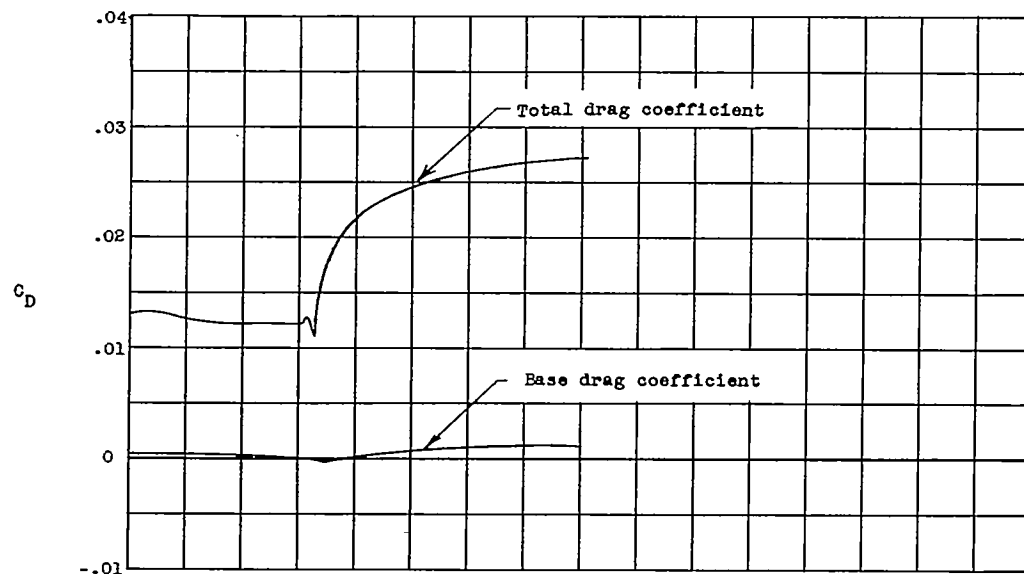
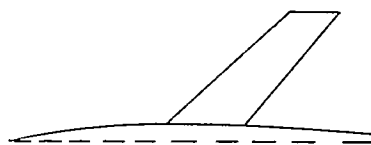
Figure 8.- Continued.

~~CONFIDENTIAL~~



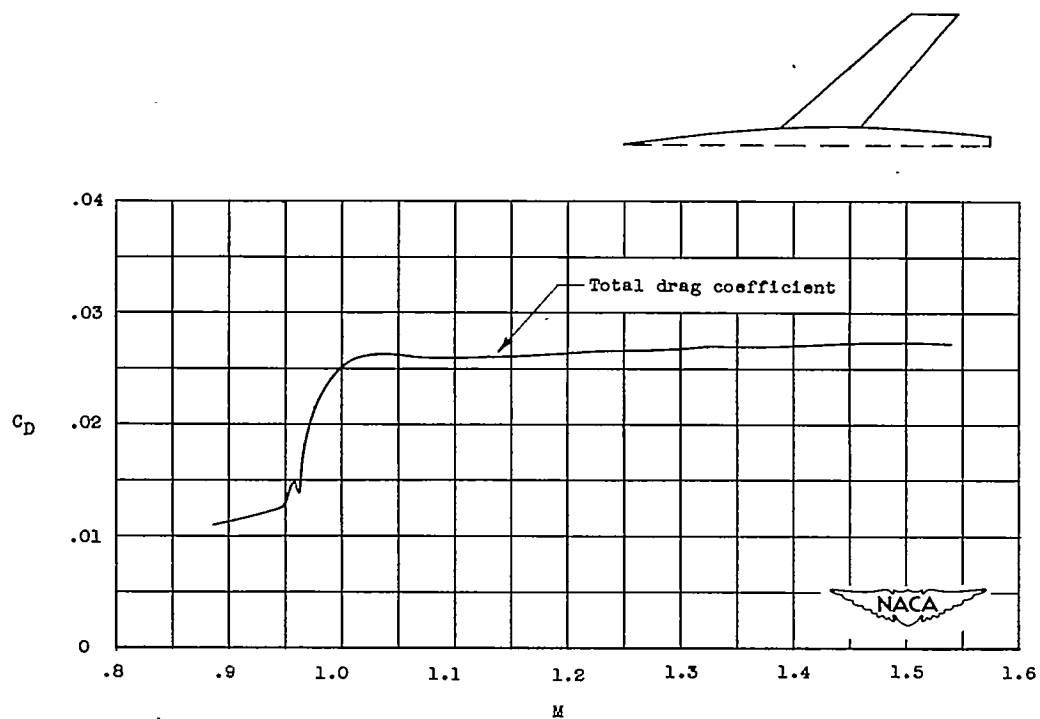
(g) Model 6.

Figure 8.- Continued.



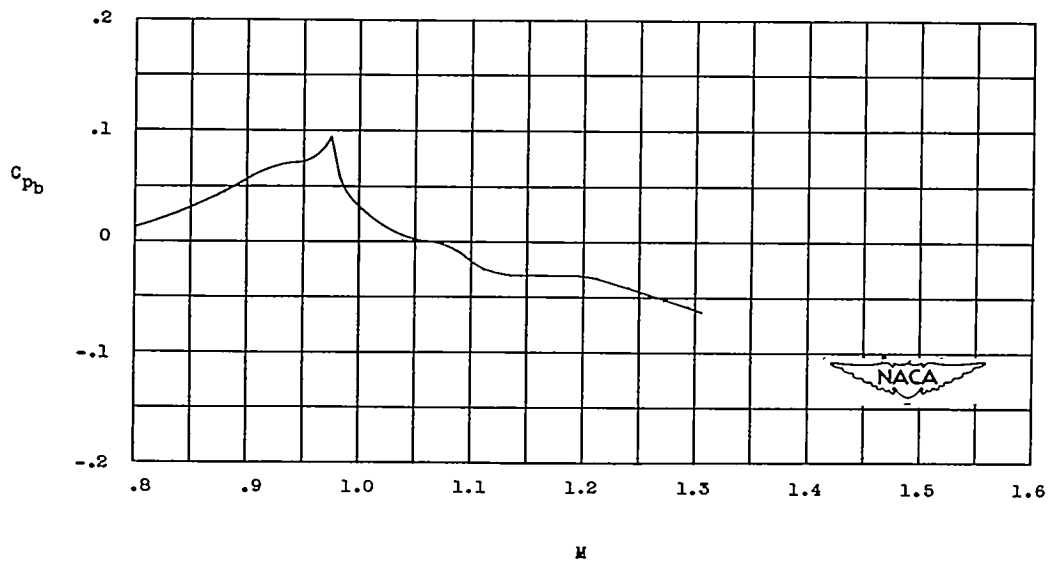
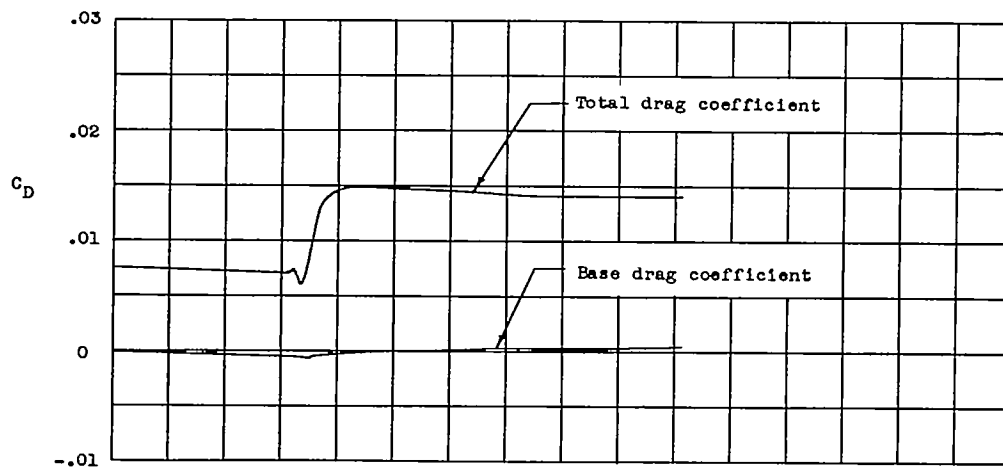
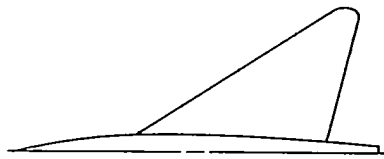
(h) Model 6a.

Figure 8.- Continued.



(i) Model 7 (reference 5).

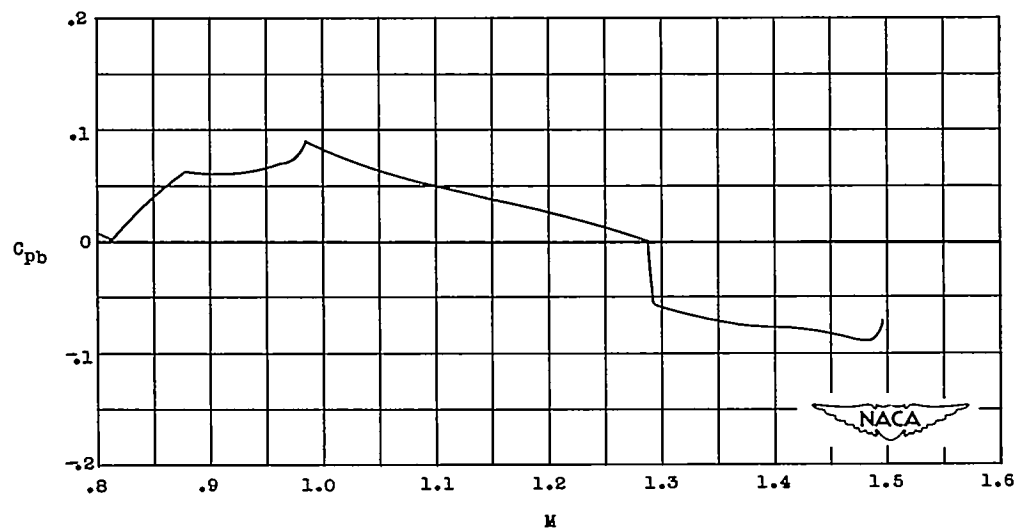
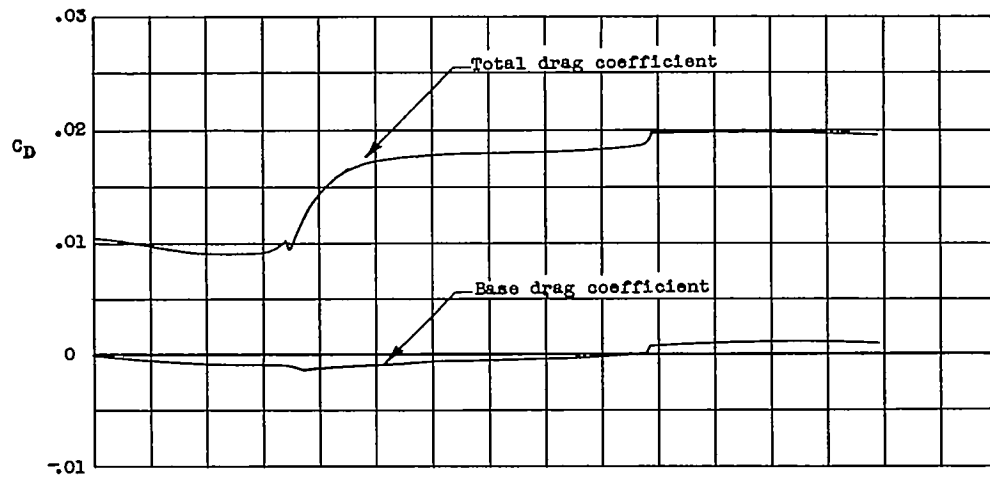
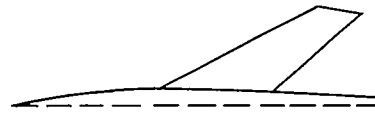
Figure 8.- Continued.

~~CONFIDENTIAL~~

(j) Model 8 (reference 6).

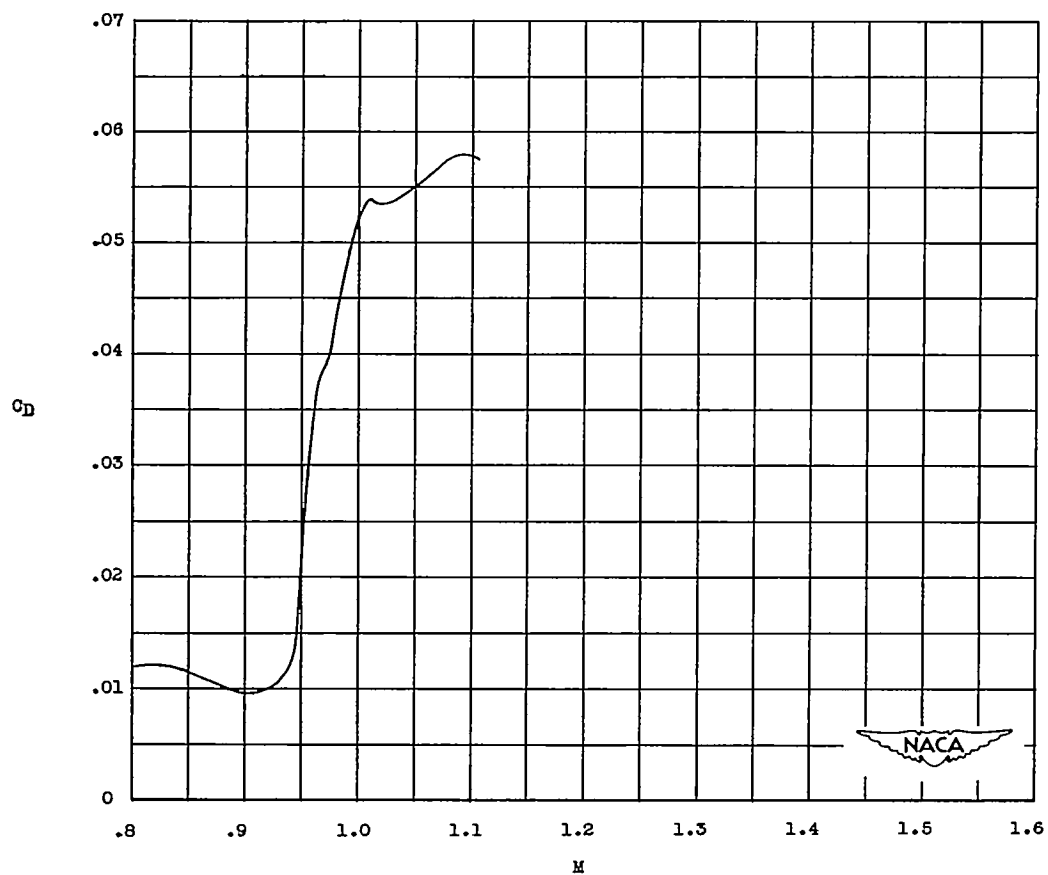
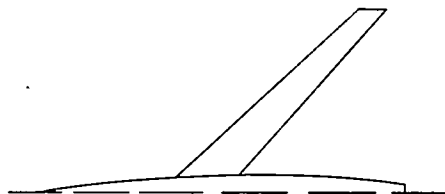
Figure 8.- Continued.

~~CONFIDENTIAL~~



(k) Model 9 (reference 7).

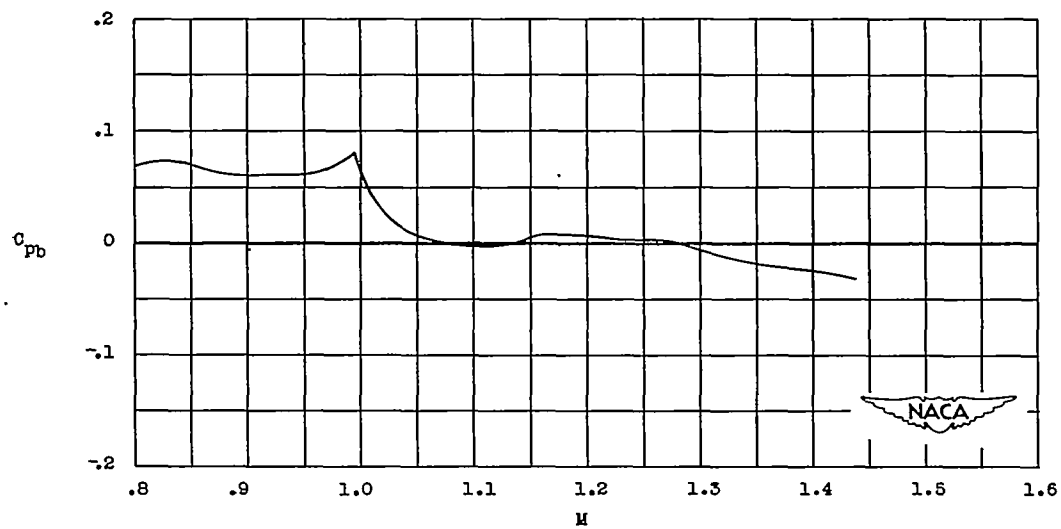
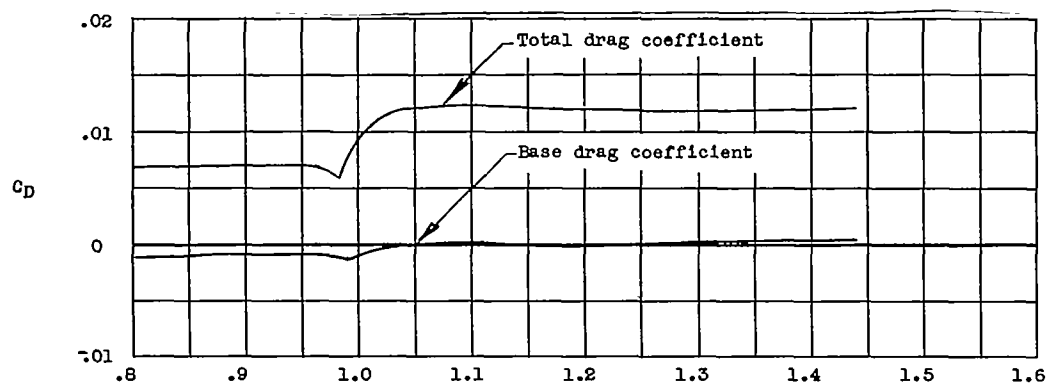
Figure 8.- Continued.

~~CONFIDENTIAL~~

(1) Model 10.

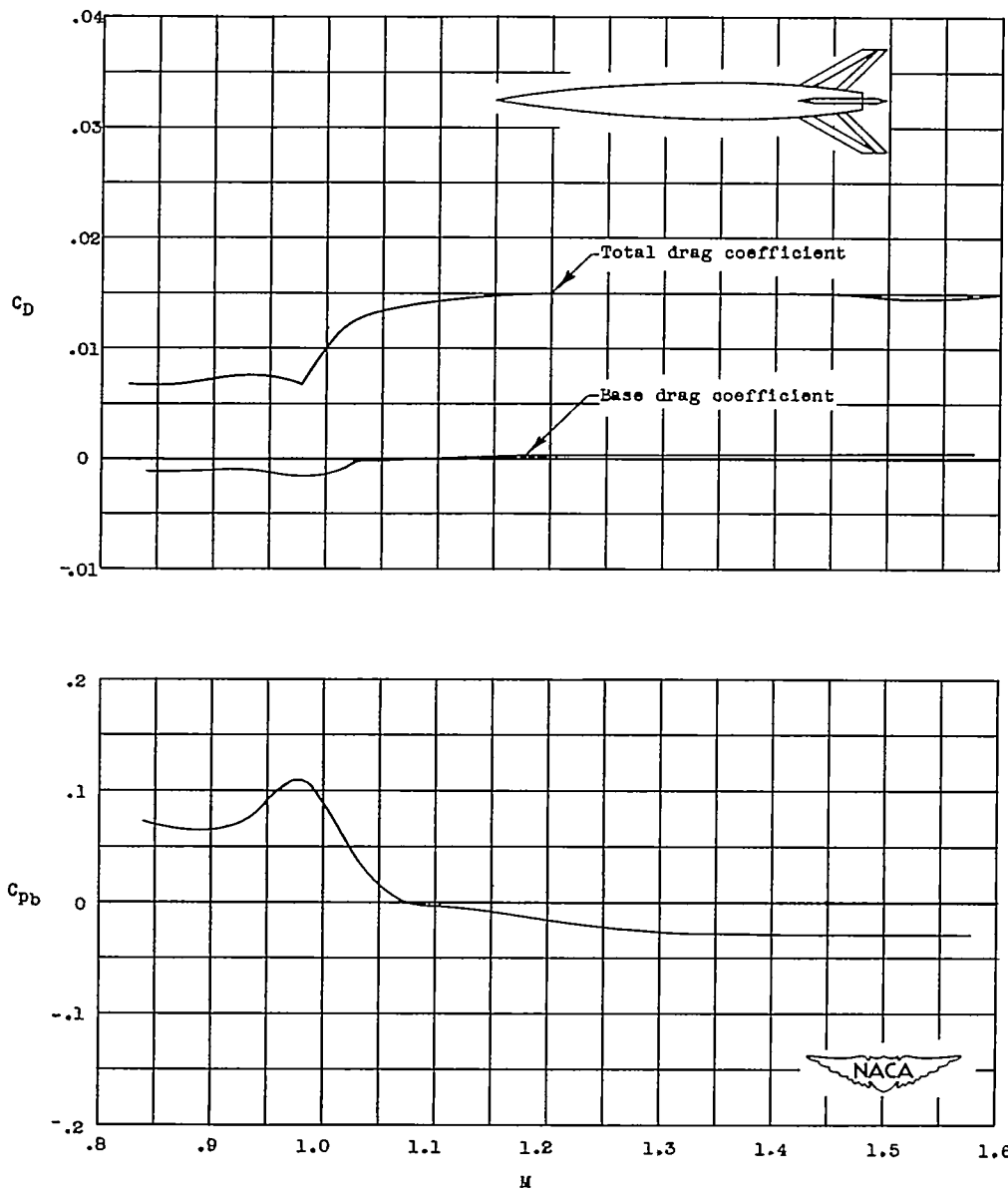
Figure 8.- Continued.

~~CONFIDENTIAL~~



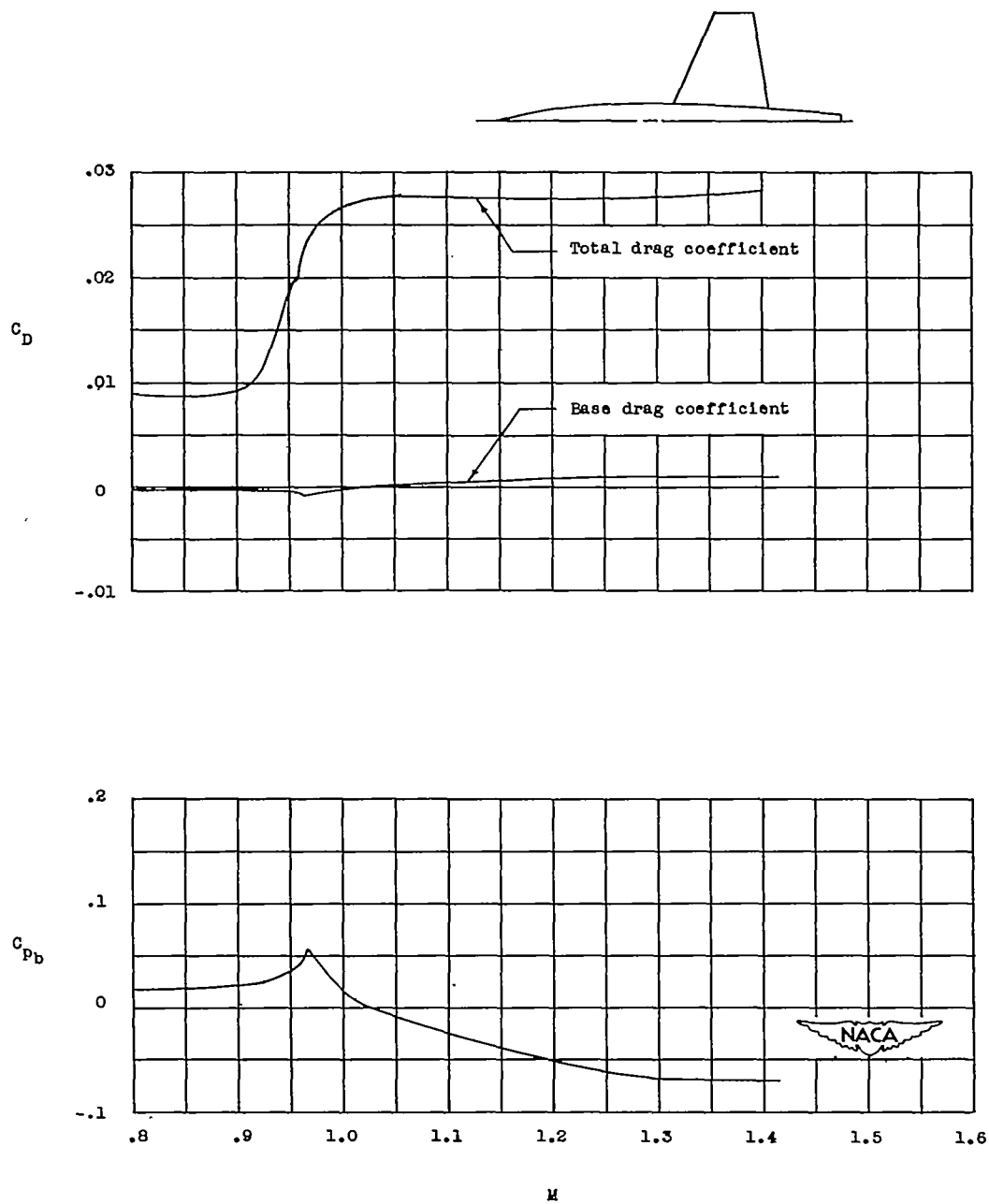
(m) Model 11.

Figure 8.- Continued.



(n) Model 11a (reference 5).

Figure 8.- Continued.



(o) Model 12.

Figure 8.- Concluded.

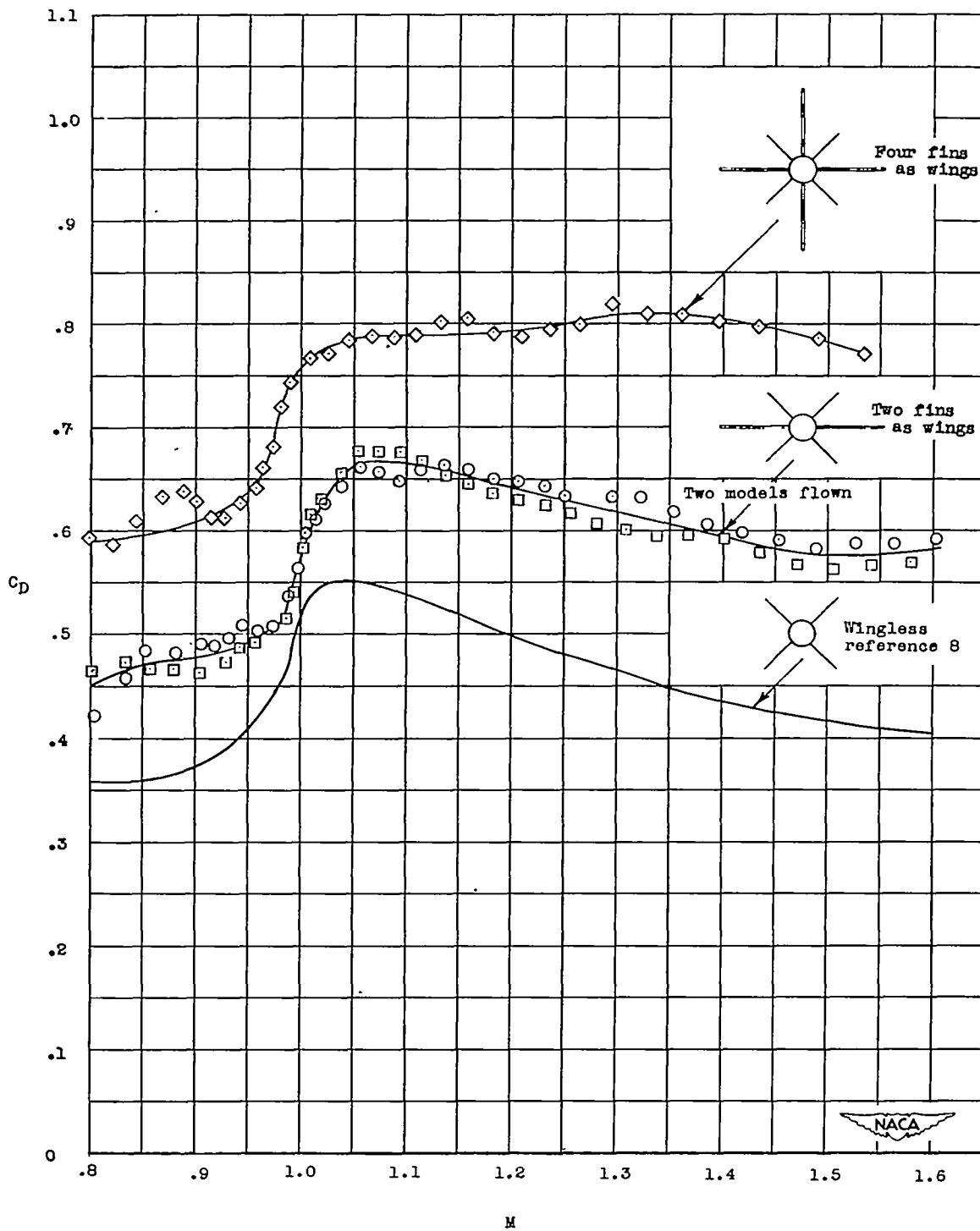


Figure 9.- Basic data for obtaining fin drag. C_D is based on body frontal area of 0.136 square foot.

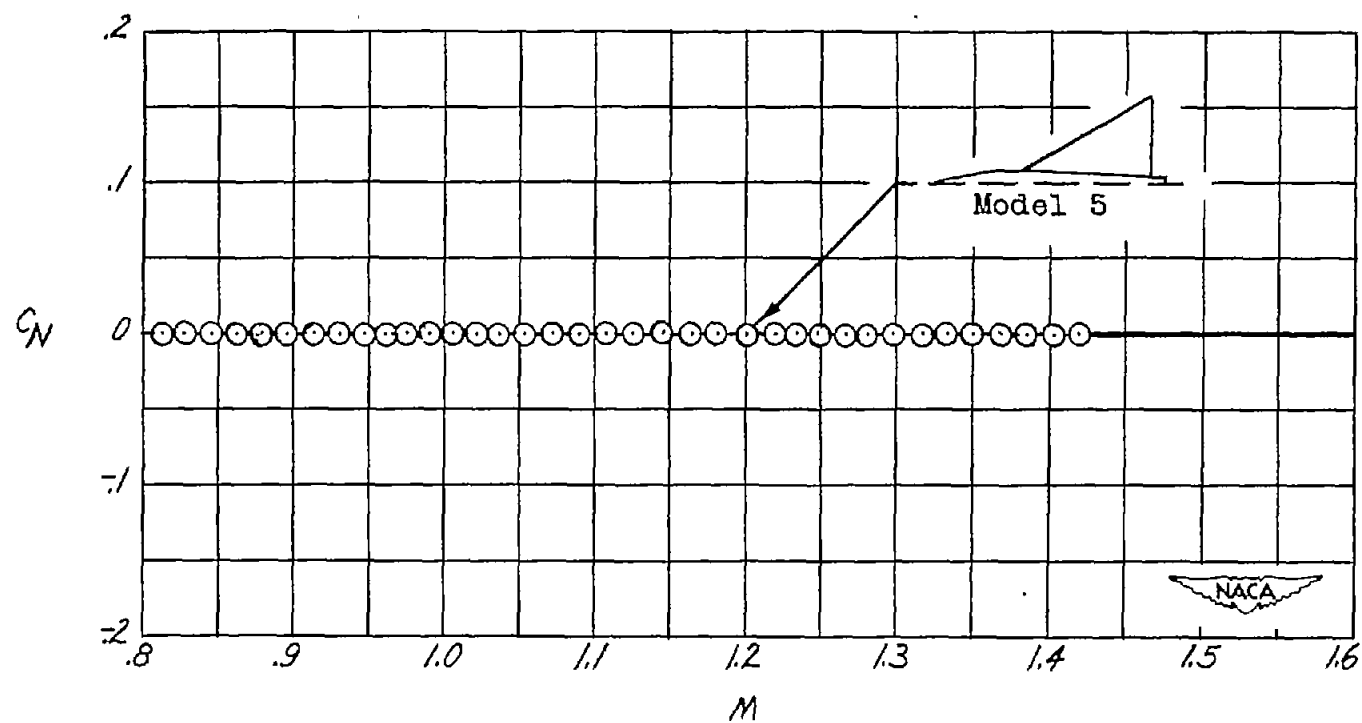


Figure 10.- Variation of normal-force coefficient with Mach number for model with large 6-percent-thick delta wing.

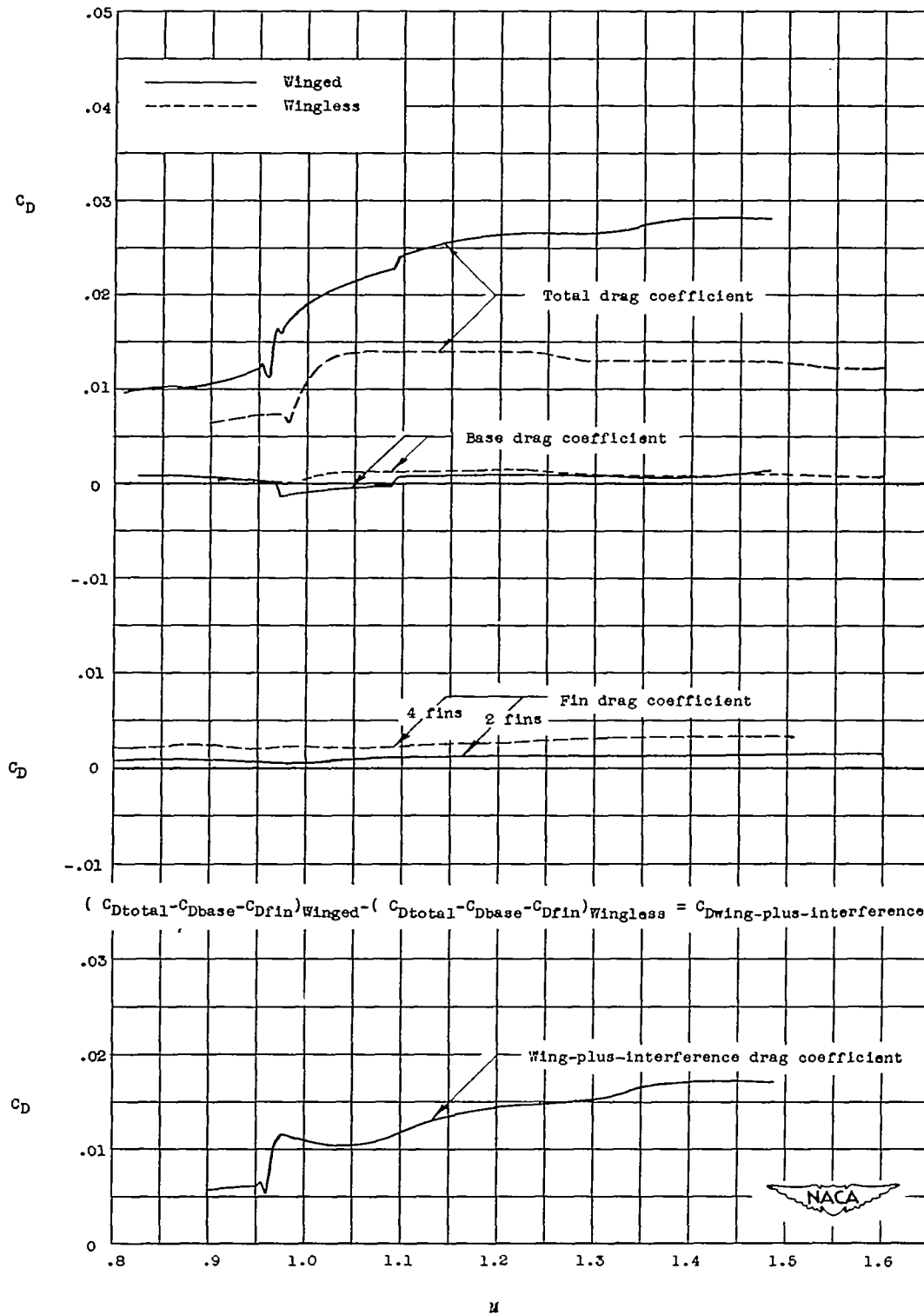
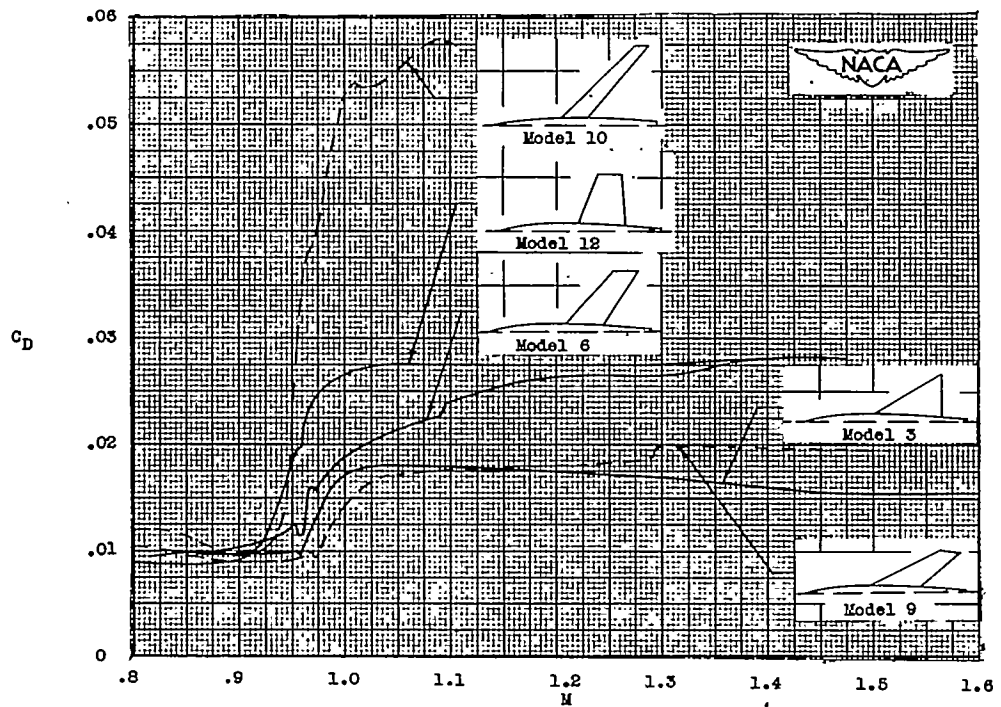
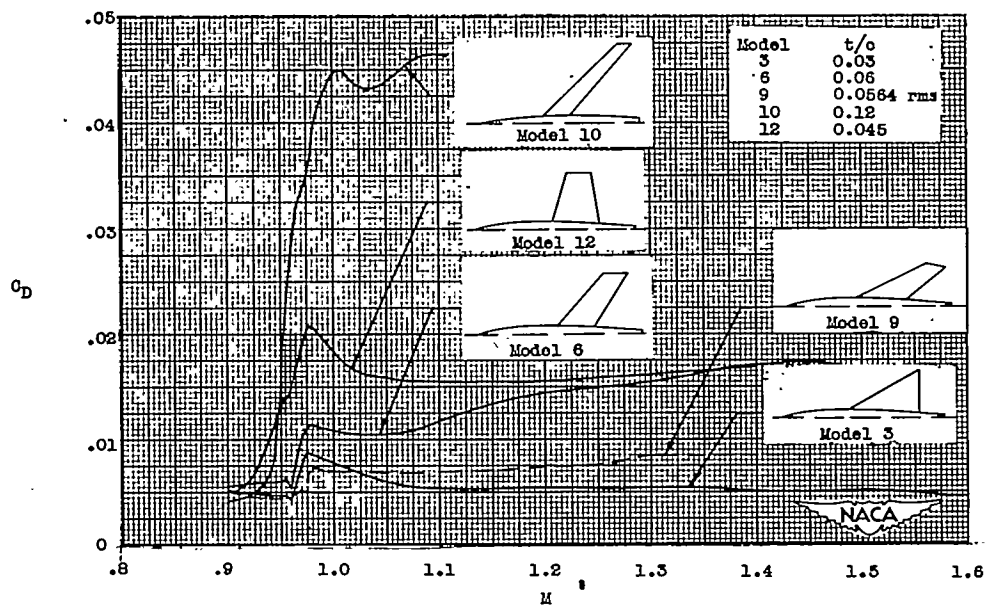


Figure 11.- Determination of wing-plus-interference drag coefficient.
Results are shown for model 6.



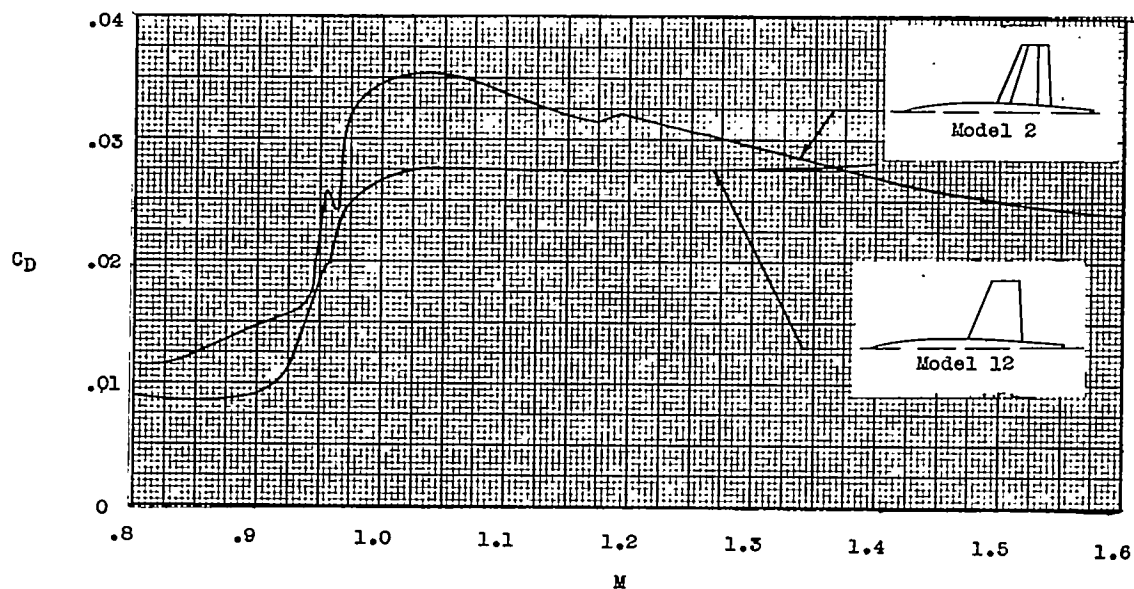
(a) Total-configuration drag coefficient.



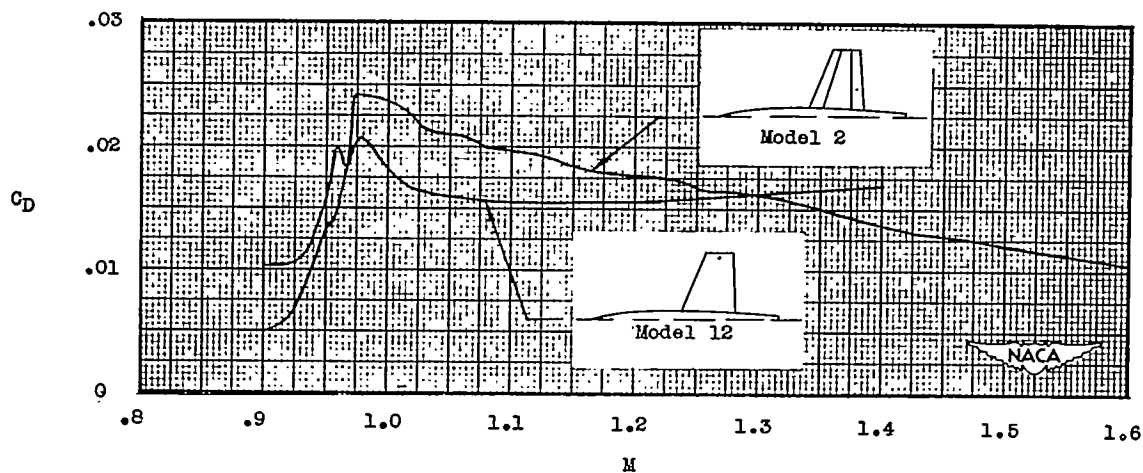
(b) Wing-plus-interference drag coefficient.

Figure 12.- Comparison of results for models having wings of equal area

$$\frac{S_f}{S_w} = 0.0606.$$

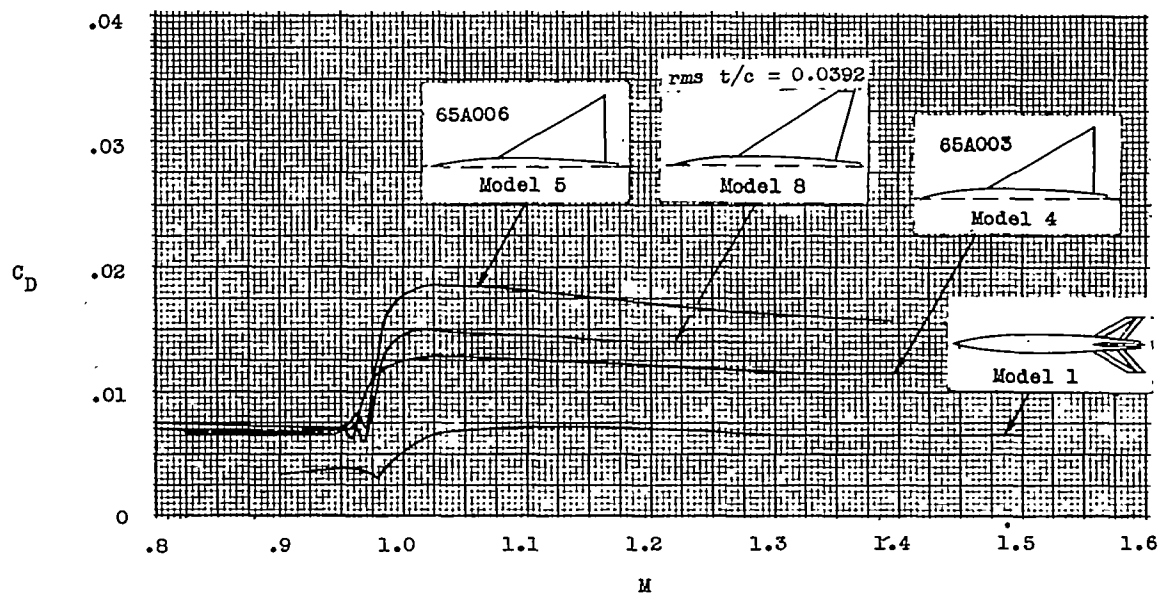


(a) Total-configuration drag coefficient.

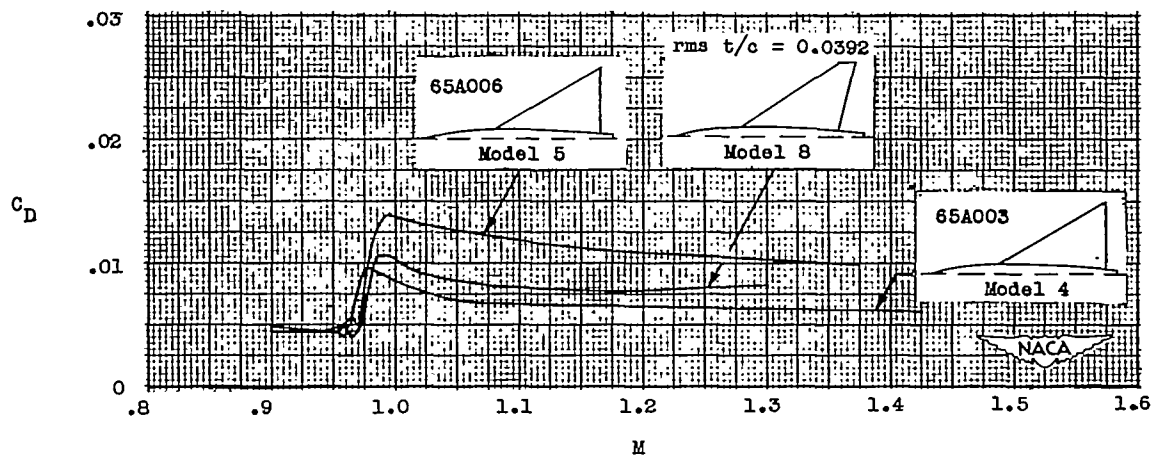


(b) Wing-plus-interference drag coefficient.

Figure 13.- Effect of changing airfoil from 4.5-percent-thick hexagonal to NACA 65A004.5 section for identical straight wings.

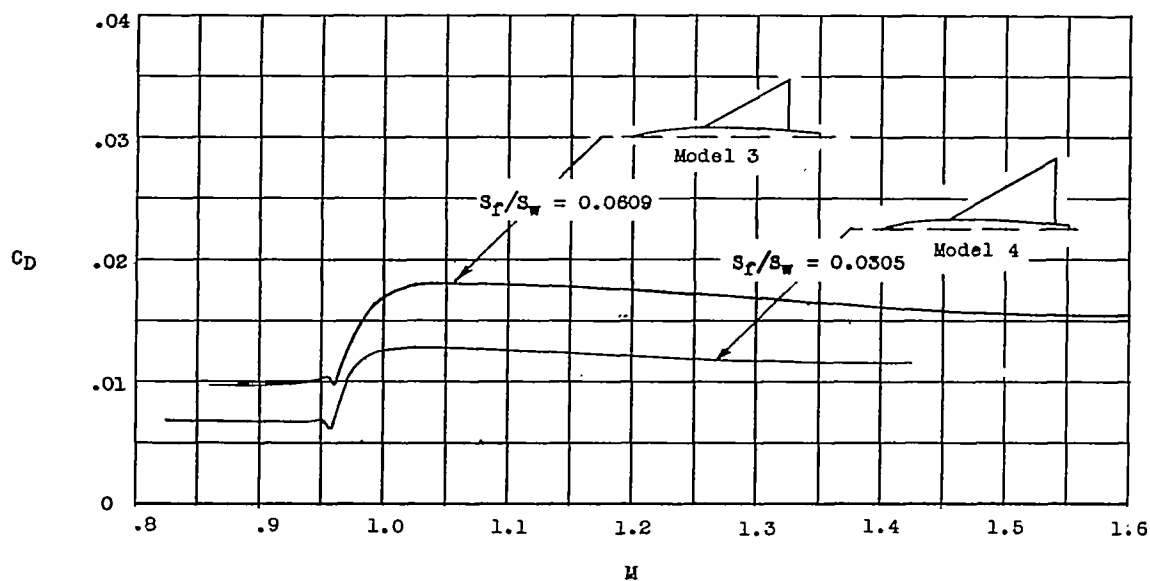


(a) Total-configuration drag coefficient.

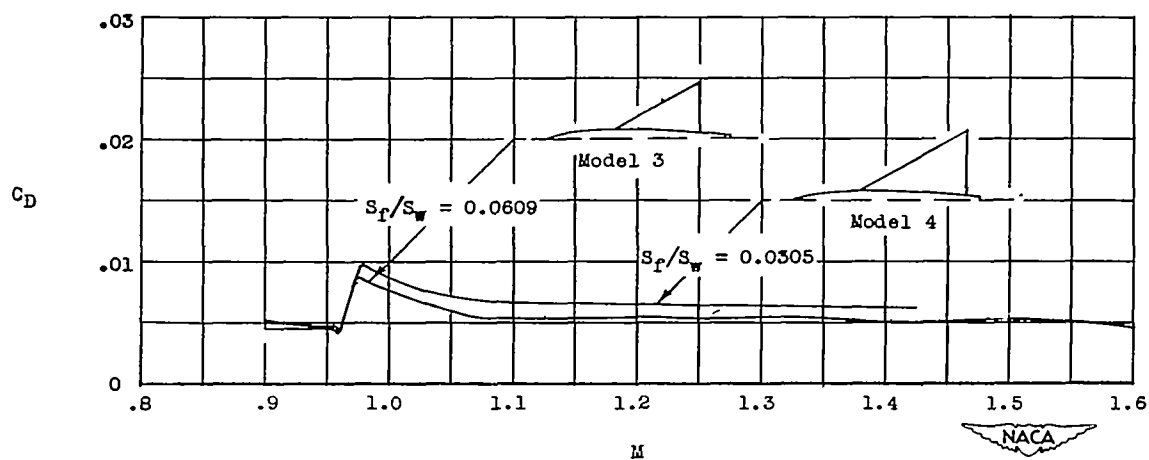


(b) Wing-plus-interference drag coefficient.

Figure 14.- Effect of wing thickness on drag coefficient for configurations having triangular wings. $\frac{S_F}{S_W} = 0.0305$.

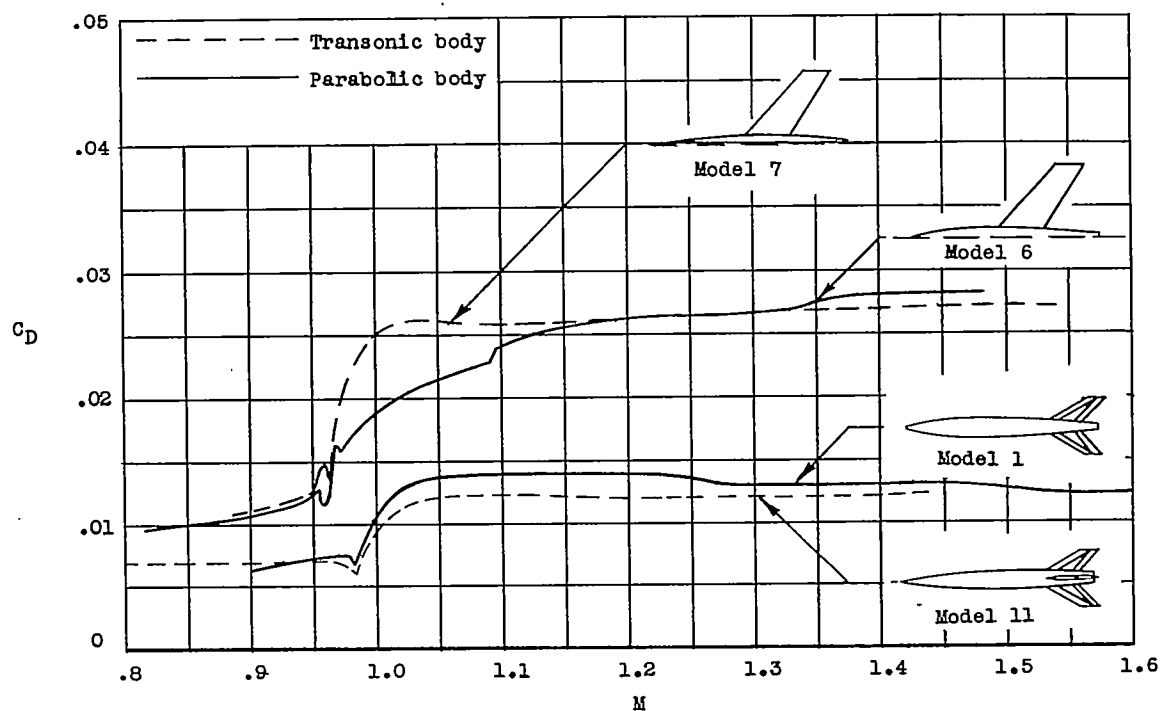


(a) Total-configuration drag coefficient.

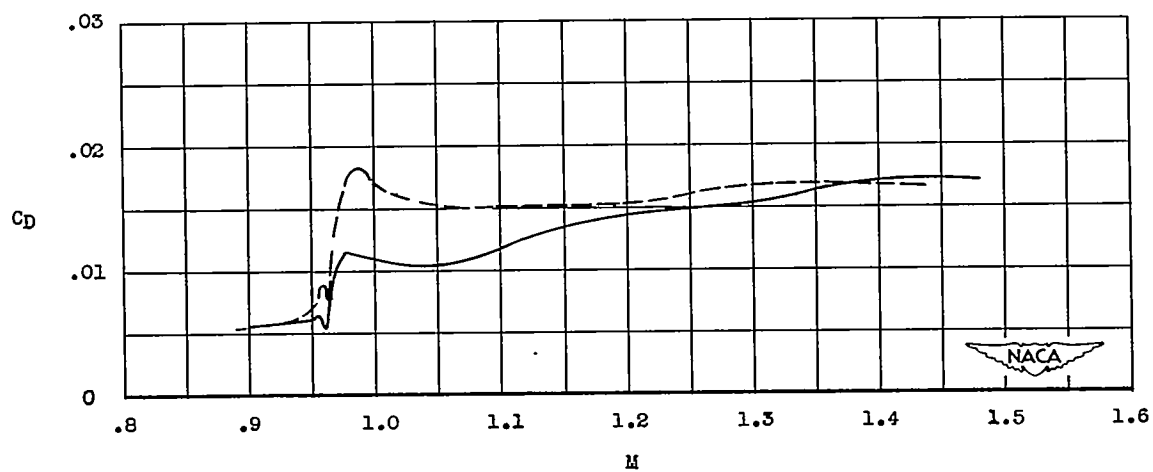


(b) Wing-plus-interference drag coefficient.

Figure 15.- Effect of body-wing area ratio on drag coefficient for models with delta wings. NACA 65A003 airfoil sections.

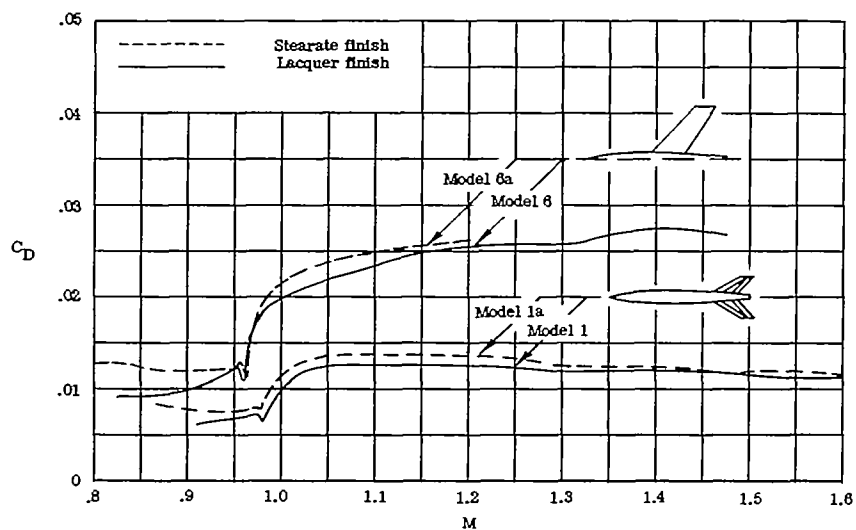


(a) Total-configuration drag coefficient.

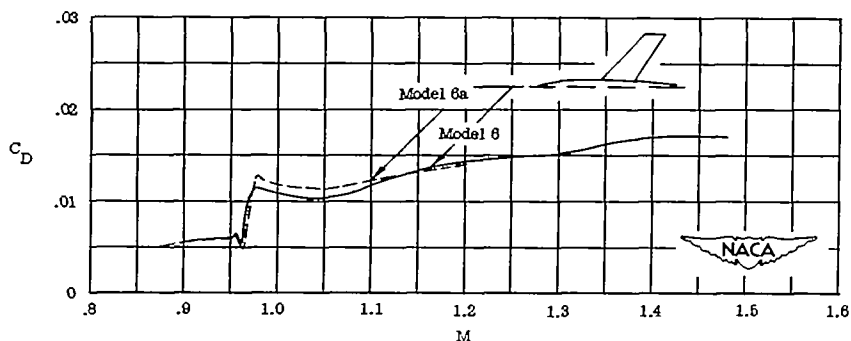


(b) Wing-plus-interference drag coefficient.

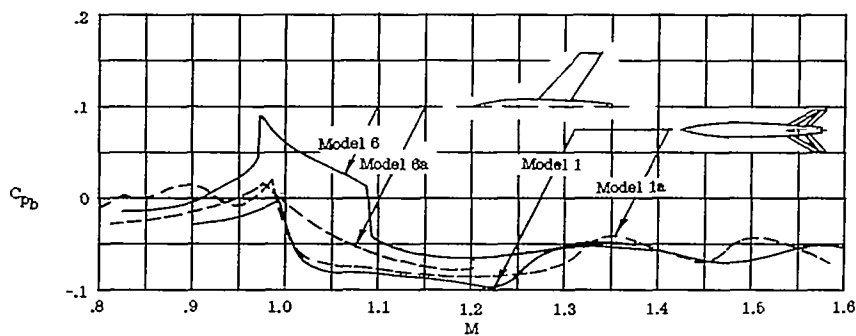
Figure 16.- Effect of body shape on drag coefficient for bodies with identical swept wings.



(a) Fore drag coefficient (total drag - base drag).



(b) Wing-plus-interference drag coefficient.



(c) Base-pressure coefficient.

Figure 17.- Effect of finish on the drag and base pressure of a vehicle with wing having 45° sweepback, 65A006 airfoil section, and taper ratio of 0.6.

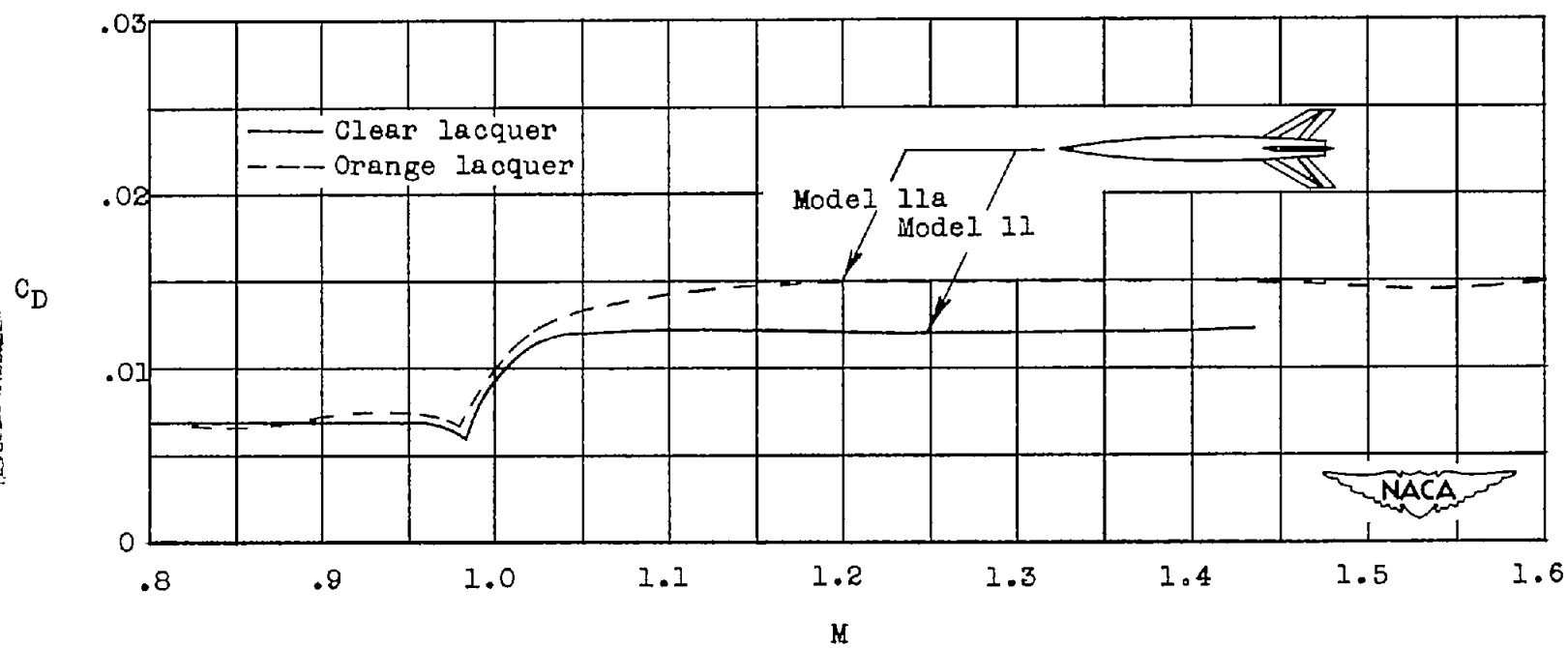


Figure 18.- Effects of finish deterioration on drag for transonic body.

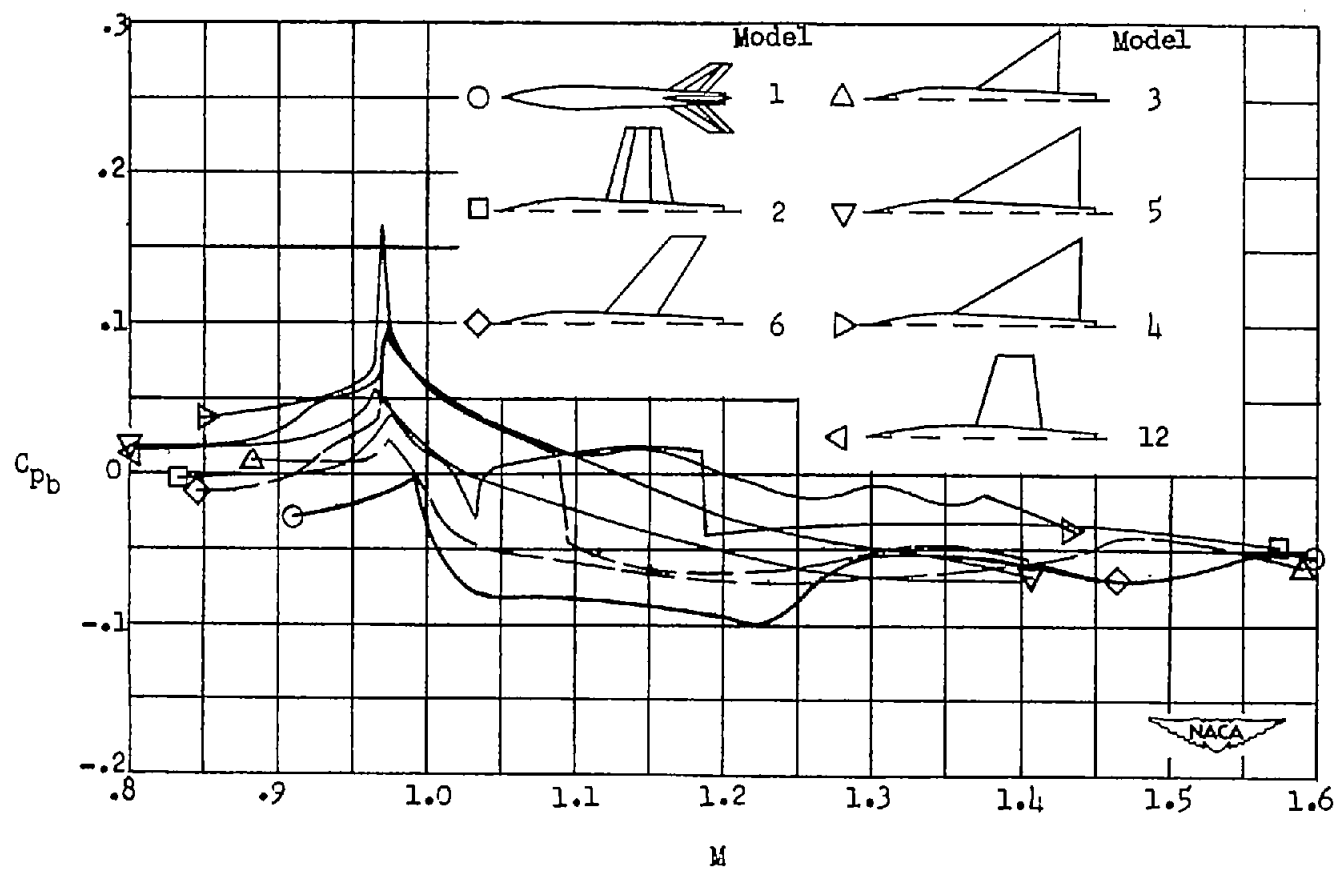


Figure 19.- Comparison of base-pressure coefficients for winged models.

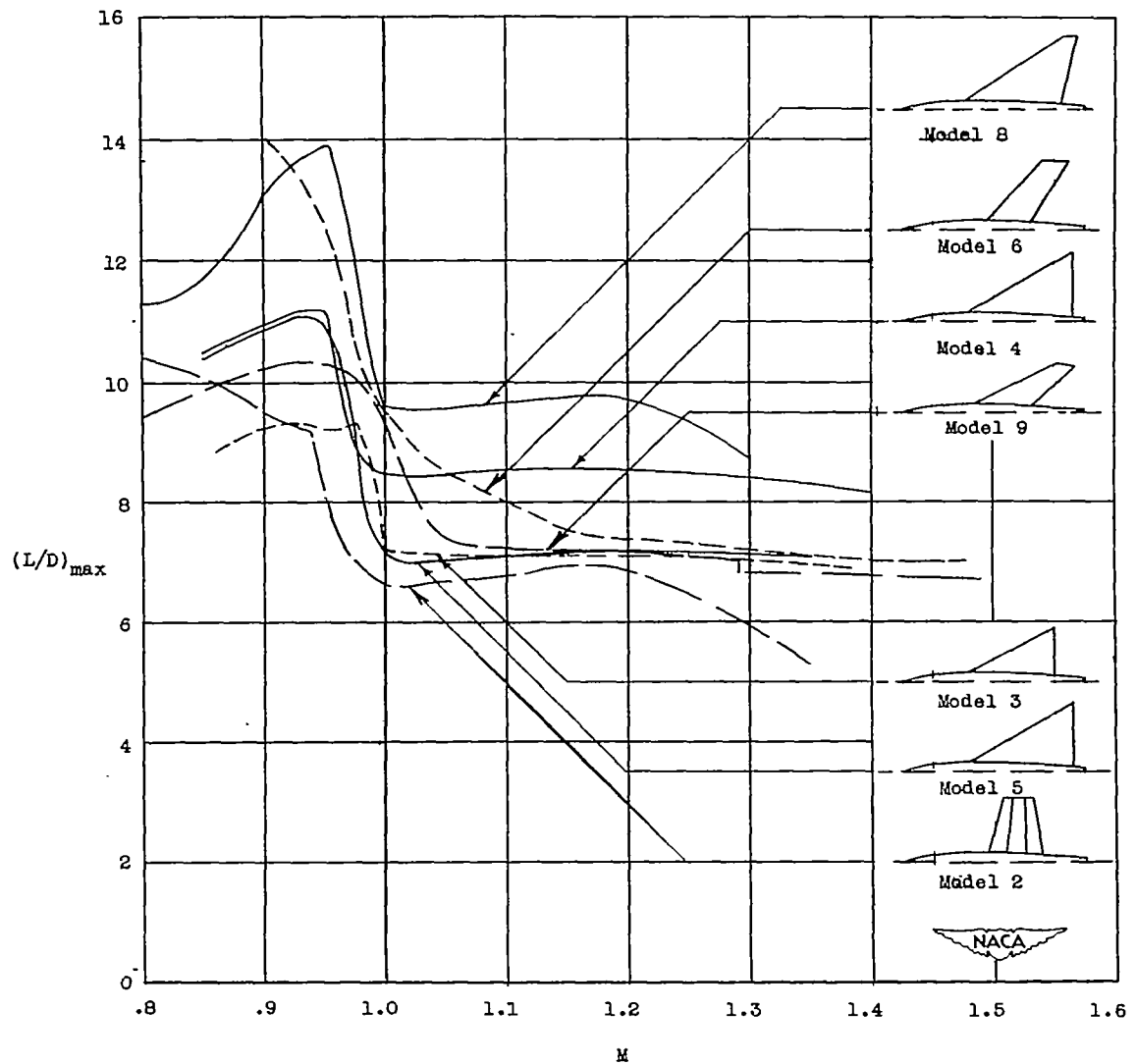


Figure 20.- Comparison of maximum lift-drag ratios.

~~CONFIDENTIAL~~